SEASONAL VARIATIONS OF AIR MASSES IN THE ARCTIC AND IN THE MIDDLE AND HIGH LATITUDES OF THE EASTERN PART OF THE EURASIAN CONTINENT

Hiromitsu KANNO*

Abstract The seasonal variations of stratification and distribution of air masses in the Arctic and the middle and high latitudes in the eastern part of the Eurasian Continent were examined. The Arctic, the eastern part of the Eurasian Continent, the Sea of Okhotsk, and the Bering Sea were selected for the important airmass source regions. By using the seasonal variations of airmass stratifications, which tend to be changed simultaneously, the year 1985 was divided into five stages. The schematic models of air masses and frontal zones in each stage — stage I: late October to late February, stage II: early March to the first half of April, stage III: second half of April to early June, stage IV: mid-June to late August, stage V: early September to mid-October — are presented.

Key words: air mass, vertical structure, seasonal variation, frontal zone

1. Introduction

An air mass is a large body of air with relatively homogeneous properties across its horizontal extent. Since the air mass causes regimes of weather, such as cold polar outbreaks in winter or hot, humid days in summer, the air mass is thought to be one of the important elements of climate.

Bergeron (1930) defined the air mass as a large body of air whose properties were uniform horizontally and which was formed by residing over an expansive surface until it took on the thermal and moisture characteristics of the region. A front was also formed around the boundary of air masses. Petterssen (1940) made geographical classifications of air masses and investigated their properties. Moreover, Arakawa (1943) discussed the relation between the weather and the properties of air masses.

* Department of Yamase-Area Agro-Environment, Tohoku National Agricultural Experiment Station

Thereafter, many studies of air masses have been done; the monthly airmass distributions over the Northern Hemisphere were shown by Brunnschweiler (1957), the airmass source regions and frontal zones over the globe are described by Willett and Sanders (1959), the relation between the air masses and the boreal forest over North America was investigated by Bryson (1966) and Barry (1967), and the connection between the Arctic front and the tundra-taiga boundary in Eurasia was examined by Krebs and Barry (1970). Furthermore, Wendland and Bryson (1981) investigated the airstream source regions, and suggested the close relationship between the air masses and the airstreams.

However, two important problems are found in the previous airmass studies. One is incomplete understanding of the vertical structure of air masses. Although the vertical profile of temperature and mixing ratio at representative stations were shown by Petterssen (1940) and Arakawa (1943), the height of the air masses was not discussed. Also, Sugimoto (1966), Kato (1985, 1987), and Kanno (1988) indicated the detailed vertical structure of air masses; however, the area (East Asia) and the season (the Bai-u season) were limited.

The second problem is that the airmass distributions and variations through the year are not known. This is due to the absence of studies of air masses in spring and autumn. Although Brunnschweiler (1957) showed monthly airmass distributions in the Northern Hemisphere, they are not common because they are divided too small.

Therefore, the description of air masses in recent meteorological and climatological textbooks (*e.g.*, Henderson-Sellers and Robinson, 1986; Barry and Chorley, 1987; Nitta, 1988) still describe the same concept of air masses as in the 1940's, and do not show the three-dimensional properties and the distributions of air masses in spring and autumn. Also, the correspondence between air masses defined by using the temperature and water vapor amount on isobaric surfaces (*e.g.*, Saito, 1966; Matsumoto *et al.*, 1971) or recognized on vertical cross-sections (*e.g.*, Palmén and Newton, 1969; Ogawa, 1987) and air masses which are geographically divided are still not fully inspected.

On the other hand, many studies in meteorology and climatology indicate that sub-seasons shorter than the four seasons are important for analyzing atmospheric phenomena. For example, Yoshino (1963, 1965) divided the early-summer rainy-season over East Asia into four stages by considering the positions of frontal zones and westerly winds at the 500 mb level. Kato (1985, 1987) examined the evolution of the Bai-u frontal zone and the air mass transformation in late May over China. Kato (1989) also investigated the seasonal transition of the characteristics of the low-level circulation systems around the Bai-u front in China from spring to summer and their relationship with the Northern Summer Monsoon (Kato, 1989). Kanno (1988) showed the relation between the polar air mass and the Bai-u front over East Asia in considering the four stages of the Bai-u season. Matsumoto (1988) divided the period from late summer to autumn into four stages and examined the large-scale atmospheric situation over East Asia. Moreover, some natural seasons and singularities in Japan were expressed by using the normals of meteorological elements (*e.g.*, Takahashi, 1942; Saito, 1957; Maejima, 1967; Yoshino and Fukuoka, 1967; Itokazu, 1972; Kawamura, 1973). The seasons in the upper and middle troposphere were also examined (Kimachi, 1953; Tamiya, 1986).

Therefore, the sub-seasons are needed to study the annual variations of airmass properties.

Besides, while the positions of frontal zones over the Northern Hemisphere were investigated (*e.g.*, Schumann and van Rooy, 1951; Reed, 1960; Yoshimura, 1967), the relationships between the air masses and frontal zones were not fully examined. Matsumoto (1983) indicated the position of the wintertime Arctic frontal zone by using three-dimensional frontal analysis; however, the properties of Arctic air masses were not analyzed. Consequently, the relationships between the airmass distributions and frontal zones remain indistinct.

This study aims to clarify the vertical structures and distributions of air masses, and their seasonal variations in the Arctic and in the middle and high latitudes of the eastern part of the Eurasian Continent. The relationships between the airmass distributions and frontal zones are also investigated.

2. Data and Analysis Procedures

The critical properties of an air mass are temperature, humidity, and lapse rate. Of these, temperature and humidity are largely influenced by the surface over which an air mass originates, whereas lapse rate is controlled by a number of factors. For example, features of the general circulation, such as the subtropical high pressure system or the intertropical convergence zone, determine the lapse rate of an air mass (Corcoran, 1987).

On the other hand, a strong wintertime ground inversion in the Arctic and its influence on the Arctic front were discussed by Kikuchi (1979). Also, Kato (1985) investigated the development of a mixed layer of 2000-3000 m thickness through dry convection caused by sensible heat from the ground over China. Their results imply that the surface air-temperature determines the lapse rate of an air mass in middle and high latitudes of the Northern Hemisphere except for the subtropical high-pressure cells. So, the large body of air formed by heating and/or cooling from the surface with horizontally homogeneous properties is regarded as the 'air mass' in this study. The airmass source regions are used for naming the air mass, that is, the air mass located in the Arctic is defined as the 'Arctic air mass' in spite of the season, and then its seasonal variation due to the thermal influences of the surface are investigated. The way that the physical features of an air mass are described and the way that an air mass in one source region is changed by the seasons (for example, the air mass located in the Arctic in winter is defined as the Arctic air mass and in summer is considered the polar air mass) was indicated by Brunnschweiler (1957). However, before using such a concept, the seasonal variations of the surface thermal characteristics must be investigated. The data and analysis procedures used in this study are as follows.

First, the airmass source regions were defined by considering the monthly mean surface air temperatures in January and July, from 1931 to 1960 (from 1951 to 1980 in Japan) compiled by the World Meteorological Organization. The study area was north of 20°N in the Northern Hemisphere, and 742 meteorological stations were used. Since the temperature lapse-rate could not be assumed from the mean temperatures, an altitudinal

revision was not executed. Over the oceans and the Greenland, the isotherms were interpolated by the values of surrounding stations, because of a few meteorological stations in them.

Next, the vertical structures of air masses were investigated by using "SD Data" (Sorted Data), which was the upper air observation data compiled by the forecasting division of the Japan Meteorological Agency (JMA). Since no unusual weather and a quite normal seasonal variation were observed in Japan, the year 1985 was selected for the analysis. The meteorological observation stations with nearly complete data in each airmass source region were selected. In order to eliminate the diurnal and transient variations and regional differences, the data twice daily (00 and 12GMT) were averaged in each airmass source region every 5 days at the mandatory levels (500, 700, 850 mb, and surface). The seasonal variations of airmass stratifications were investigated by using the surface potential temperature, equivalent potential temperature (θe), mixing ratio, and the vertical differences of θe. The year 1985 was divided into several stages in consideration of the above results, and the airmass stratifications in each stage were examined.

Furthermore, airmass boundaries were investigated by using the time-latitude cross-sections made by "GA Data" (Global Analysis Data), which was compiled in the form of 2.5° latitude-longitude grid produced by the forecasting division of JMA. In order to eliminate local differences, these grid data were averaged for every 20-degrees of longitude (90-110°E and 140-160°E).

Lastly, the frontal zones were distinguished by using the synoptic charts published by Deutscher Wetterdienst, and compared with the airmass boundaries in each stage. The vertical structures of fronts and air masses were analyzed based on the vertical cross-sections along meridians. The schematic model of air masses and frontal zones in the Arctic and in the middle and high latitudes of the eastern part of the Eurasian Continent are presented in chapter 8.

3. Airmass Source Regions over the Northern Hemisphere

Figure 1 depicts the distribution of monthly mean surface air temperatures in January and July. The important airmass source regions are defined as areas in which the horizontal temperature gradient is relatively small and/or the temperature is extremely low.

In January, an extremely low-temperature area, less than −40°C, is found in the northeastern part of the Eurasian Continent. While the temperature gradient is not small, this area corresponds to the source region of dominant anticyclones and the properties of air — water vapor and stratification — are thought to be uniform over a vast extent. So, this area is considered as the Pc (Polar continental) airmass source region. Since the Arctic is surrounded by isotherms and the temperature gradient is small, this area is defined as the A (Arctic) airmass source region.

On the other hand, the North American Continent was considered as the Pc airmass source region by Petterssen (1940) and Willett and Sanders (1959). However, the meridi-

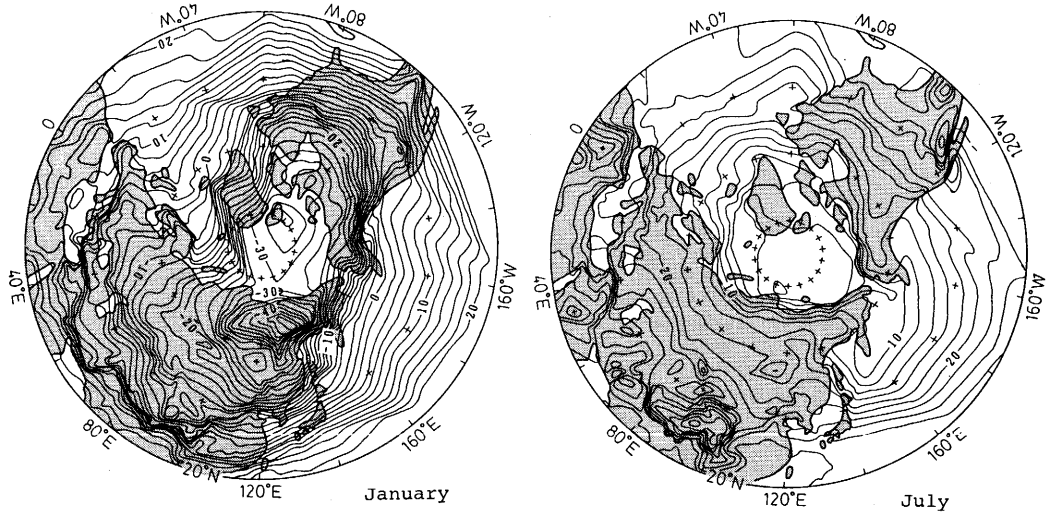

Fig. 1 Monthly mean surface air temperatures from 1931 to 1960 (from 1951 to 1980 in Japan) in January and July

onal temperature gradient is very large (Fig. 1), so an independent air mass may not be formed. Around the Bering Sea and the Sea of Okhotsk, the temperature gradient is large. So, these areas are considered as airmass modification areas.

In July, the temperature gradients are small in the Arctic and from the Bering Sea to the Sea of Okhotsk. Since these areas are surrounded by isotherms, an air mass may be formed. Then, the Arctic is defined as A airmass source region and the area from the Bering Sea to the Sea of Okhotsk is considered as the Pm (Polar maritime) airmass source region. Also, the temperature gradient on the Eurasian Continent is small, so this area is defined as the Pc airmass source region.

Around the periphery of the Arctic Ocean, especially between 80°E and 160°E, the temperature gradient is large; this is considered as the boundary between the A air mass and the Pc air mass.

On the other hand, the temperature gradient is small in the northwestern part of North America. However, this area is a mountainous region — the Alaska Range, Coastal Mountains, and Rocky Mountains, so the airmass analysis is difficult. Therefore, this area is excluded from the study area. Also, Petterssen (1940) defined the northern part of the North American Continent as the Pc airmass source region, and Willett and Sanders (1959) considered it the cPK (colder Polar Continental) airmass source region. However, since the meridional temperature gradient is not small, that area are not recognized as an airmass source region in this study.

In consequence, the Arctic, the eastern part of the Eurasian Continent, the Sea of Okhotsk and the Bering Sea are defined as airmass source regions. Figure 2 shows the selected meteorological observation stations in each airmass source region. Four stations in the Arctic, five stations in the eastern part of the Eurasian Continent (south of 65°N), six stations in the Sea of Okhotsk and six stations in the Bering Sea were selected for airmass analysis. The Sea of Okhotsk and the Bering Sea are analyzed separately

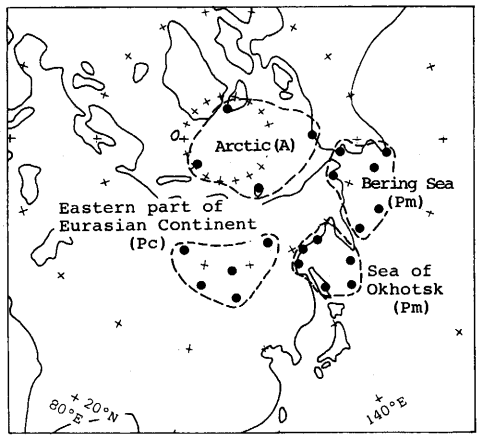

Fig. 2 Airmass source regions and upper-air observation stations used for analysis

because of their different synoptic conditions.

4. Seasonal Variations of Airmass Stratifications

Airmass stratifications in each airmass source region

The Arctic (A air mass)

Figure 3 depicts the temporal variations of surface θe, potential temperature (θ) and mixing ratio (x), and the vertical differences of θe between mandatory levels (θe_{500}-θe_{surf}, θe_{500}-θe_{850}, and θe_{850}-θe_{surf}) in each airmass source region. The θe_{500}-θe_{850} indicates the stratifications of the middle-level layer and θe_{850}-θe_{surf} indicates that of the low-level layer in the atmosphere.

The x in the Arctic indicates the least amount of other airmass source regions (Fig. 3-a), so the differences between θ and θe are small even in the warm half of the year. The θ and θe show nearly fixed values, about 250 K, from mid-December to early April, and the minimum value is seen in late March. The increases of θ and θe between mid-April and early June, and the decreases between late September and late October are at nearly constant rates.

The θe_{500}-θe_{surf} discontinuously falls in mid-April and early June and rises from mid- to late October. Consequently, the atmospheric stability below the 500 mb level is relatively small between early June and late October.

Compared with the difference between θe_{500}-θe_{850} and θe_{850}-θe_{surf} from early September to late October, that from early June to late August is relatively small. Also, θe_{850}-θe_{surf} tentatively becomes larger than θe_{500}-θe_{850} in the period from early June to late August. Consequently, the stratification in the low-level layer between early June and late August is more stable, and is regarded as a different stratification from that between early September and late October.

In these circumstances, the stratification in the Arctic discontinuously changes in mid-April, early June, early September and late October (shadings in Fig. 3-a). Among these periods the stratification is regarded as nearly uniform. Compared with the

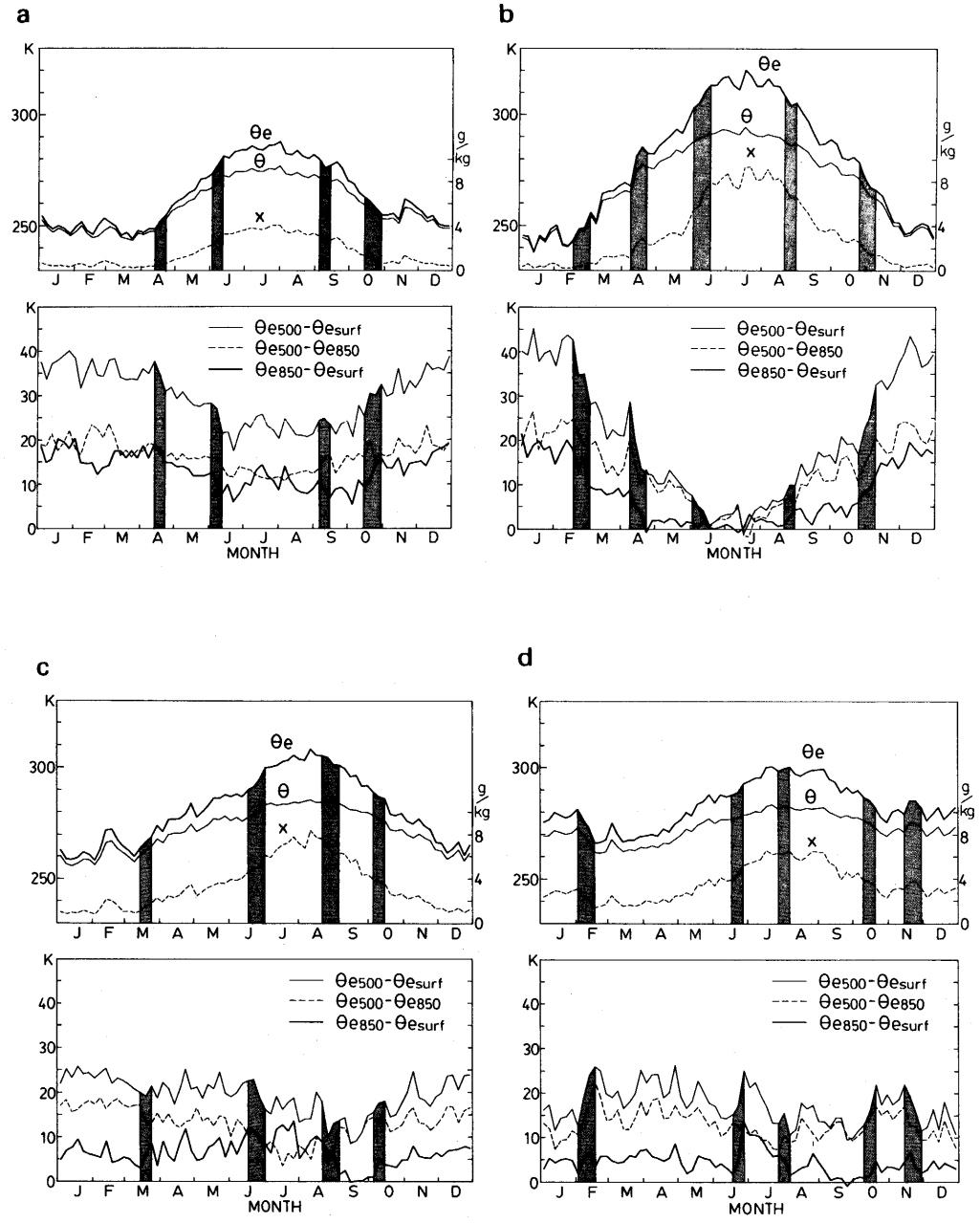

Fig. 3 Temporal variations of surface equivalent potential temperature, potential temperature and mixing ratio (upper) and the vertical differences of equivalent potential temperature between mandatory levels (lower) in each airmass source region in 1985
a : Arctic, b : Eurasian Continent, c : Sea of Okhotsk, d : Bering Sea, θe : equivalent potential temperature, θ : potential temperature, x : mixing ratio
Shadings indicate changing periods of stratifications.

temporal variations of surface meteorological elements, mid-April, early June, and early September nearly correspond to the inflection points of those variations. Therefore, the stratification in the Arctic seems to be largely influenced by the surface thermal conditions.

The eastern part of the Eurasian Continent (Pc air mass)

Since surface x is large, the difference between θ and θe is large from late May to mid-September (Fig. 3-b). While θ and θe begin rising in late February, it is one month earlier than that in the Arctic.

The θe_{500}-θe_{surf} is above 30 K between early November and late February, so the stratification is quite stable in this period. From early June to late August it is under 10 K and the stability becomes small.

The θe_{850}-θe_{surf} discontinuously falls in late February and mid-April, and rises from late October to early November. It is under 5 K between mid-April and late August, so the stability in the low-level layer is very small in this period. Besides, while abrupt changes are not found in the middle-level layer (θe_{500}-θe_{850}), the stability is low between early June and late August.

Therefore, the stratification in the eastern part of the Eurasian Continent changes in late February, mid-April, early June, late August and from late October to early November. Compared with the temporal variations of surface θ, θe and x, early February corresponds to the beginning of risings of θ and θe and mid-April coincides with abrupt risings of them. So the rising surface temperature and falling atmospheric stability nearly correspond.

The Sea of Okhotsk (Pm air mass)

The surface meteorological elements tentatively rise in mid-February, and continuous rising begins in mid-March, which is one month earlier than that in the Arctic (Fig. 3-c). The θ and θe do not rise from late May to mid-June. It seems that the dominant anticyclones existing in this period around the Sea of Okhotsk to the Bering Sea prevent rising temperature. The annual range of θ is smaller than that in the Arctic. From early July to early September, the θ has a nearly constant value of about 280-285 K, whereas the difference between θe and θ is large with large values of x.

The θe_{500}-θe_{surf} discontinuously falls in late June. The stability in the middle-level layer (θe_{500}-θe_{850}) decreases after mid-June; however, that in the low-level layer (θe_{850}-θe_{surf}) increases and stable stratification remains until late August. After early September, θe_{500}-θe_{850} increases and θe_{850}-θe_{surf} decreases, and then the stability in the low-level layer indicates the lowest value of the year until early October. Also, after mid-March, the stability in the middle-level layer decreases and that in the low level layer increases. Therefore, the fact that the temporal variations of stabilities in the middle- and low-level layers have inverse correlation in the warm half of the year is considered a characteristic feature in this area. Besides, θe_{850}-θe_{surf} shows large fluctuations between mid-March and late August. Since such variations are not seen in the surface θe, warm air may be periodically advected above the ground in that period.

In the Sea of Okhotsk, the stratification changes in mid-March, late June, late August, and early October. Compared with the temporal variations of surface meteorological elements, the increasing stability in the low-level layer after mid-March corre-

sponds to rising θ and θe. Also, between late June and late August, the stratification in the low-level layer is stable and surface θ has a nearly constant value; this suggests that the Pm air mass is formed continuously in this period.

The Bering Sea (Pm air mass)

The x in the cold half of the year is larger than that of the other regions (Fig. 3-d). It seems that synoptic activities, such as the lows around the Aleutian area, bring a large amount of water vapor. The annual difference of θ also indicates the least value. Discontinuously falling θ and θe are seen from early to mid-February. After that, the rising rates of θ and θe increase after mid-April, which corresponds to that in the Arctic.

Since θe_{500}-θe_{surf} shows large fluctuations for the period over ten days throughout the year, the large-scale atmospheric circulation may exhibit large variations. The θe_{500}-θe_{surf} and θe_{500}-θe_{850} discontinuously rise in early February and mid-October, and fall in late November. In the low-level layer, θe_{850}-θe_{surf} abruptly rises in late June and gradually falls in early August. Between early August and early October, especially in late September, the stability becomes small in the low-level layer.

In these circumstances, the stratification in the Bering Sea changes in early February, late June, early August, mid-October and late November. Compared with the variations of surface θ, θe and x, the rising stability in the middle-level layer in early February corresponds to abrupt fallings of surface θ and θe; this suggests that cold air is advected in this period. Also, the discontinuous rising of stability in the low-level layer corresponds to the abrupt rising of surface x in late June, so the airmass properties may be changed in this period.

Division of 1985 into stages

The periods of change for airmass stratifications in each air mass source region are shown in Fig. 4. In two periods — from early to late June and from early October to early November — the stratifications simultaneously change in four airmass source regions. Also, from late August to early September, the stratifications change in the Arctic, the eastern part of the Eurasian Continent and the Sea of Okhotsk. Moreover, common changes are seen in the Arctic and the Eurasian Continent in mid-April. So, the airmass stratifications tend to change at nearly the same times. Then the year 1985 can be divided into stages and the airmass stratifications in each stage can be compared.

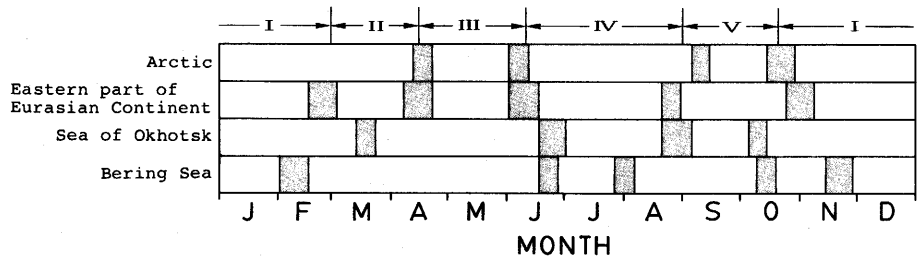

Fig. 4 Changing periods of stratifications in each airmass source region
Numerals in the upper part of figure indicate the stages in 1985.

The boundaries of the stages are defined as the period in which the airmass stratifications nearly simultaneously change. In the cold season, the variations of airmass stratification in the Sea of Okhotsk and the Bering Sea are not considered, because the Pm air mass is formed only in the warm season. Although the airmass stratification in the Arctic is not changed in late February, that in the Eurasian Continent is very apparent, so this period is selected as the boundary between stages. Accordingly, the following five stages are defined:

Stage I: October 21 to February 28
Stage II: March 1 to April 15
Stage III: April 16 to June 10
Stage IV: June 11 to August 31
Stage V: September 1 to October 20

The reason for the simultaneous change of airmass stratification is probably the discontinuous change of air mass over the continent, where large heating by solar radiation in the warm season and cooling by longwave radiation from the surface in the cold season are observed, causes a simultaneous change of the air mass in the surrounding sea areas. For example, the stable stratification in the low-level layer in the Sea of Okhotsk and the Bering Sea in stage IV may be formed by the advection of a vertically mixed, hot and humid air mass from the Eurasian Continent; that is, the advected Pc air mass is cooled by the sea surface and then the stable and shallow Pm air mass is formed. According to Borchert (1953), and Wendland and Bryson (1981), the Sea of Okhotsk and the Bering Sea are not defined as air-stream source regions. So the air masses in these regions seem to be formed secondarily and the above-mentioned hypothesis is confirmed. Also in stage V, the relatively cold air mass formed by radiative cooling from the land moves from the Eurasian Continent to the Arctic Ocean, the Sea of Okhotsk and the Bering Sea, and then it is heated by the relatively warm sea surface and the low-stability air mass is formed.

Comparisons between the stages in this study and in other studies

Table 1 lists the stages in this study and in other studies. According to Kawamura (1973), while the natural seasons have been defined by some climatologists, the results nearly correspond to each other. So, the natural seasons divided by Maejima (1967) which were classified mainly by using the daily normals were selected for comparison. Although the natural seasons were divided separately in three districts of the Japanese Islands, those in central and southwestern Japan were examined.

The winter monsoon season is specified as the period from November 28 to February 21 by Maejima (1967). On the other hand, stage I begins on October 21 and ends on February 28 in this study. While the beginnings of the winter monsoon season and stage I differ by about a month, the endings nearly correspond to each other. Since the ending of stage I contains the period in which the Pc air mass is modified, that agreement is thought to be reasonable. Also, correspondences are seen between the begining of late autumn on October 11 and the beginning of stage I on October 21, the ending of the spring season on June 12 and the ending of stage III on June 10, and the ending of midsummer on August 30 and the ending of stage IV on August 31. The ending of Bai-u season

Table 1 Stages in this study and natural seasons in other studies

	Maejima (1967)	Ninomiya and Muraki (1986)	Kanno (1988)	Matsumoto (1988)	This study
Jan.	winter monsoon season				stage I
Feb.					
	Feb. 22				Mar. 1
Mar.					stage II
Apr.	spring				Apr. 16
		pre Baiu	before Bai-u		
May					stage III
		May 21	May 27		
		early Baiu	early Bai-u		
June	June 13,14	June 11	June 21		June 11
	Bai-u season	peak Baiu	late Bai-u		
July	July 10	July 21	July 16		stage IV
	midsummer	post Baiu	after Bai-u		
Aug.				stage 1	
	Aug. 31			Sep. 6	Sep. 1
Sep.	Shurin season			stage 2	
				Sep. 27	stage V
Oct.	Oct. 11			stage 3	
	late autumn			Oct. 22	Oct. 21
Nov.				stage 4	
					stage I
Dec.	Nov. 28 winter monsoon season				

cannot be identified in this study, and the ending of stage II is not defined in Maejima (1967).

Consequently, the boundaries between the stages in this study and those of the natural seasons nearly correspond to each other in spite of the different analysis procedures and study areas. Therefore, the seasonal variations of air masses may greatly affect the climate in the Japanese Islands.

Next, Ninomiya and Muraki (1986) divided the Bai-u season in 1979 into four stages — pre-Baiu, early Baiu, peak Baiu, and post Baiu — by using the time-series of daily precipitation. The beginning of the peak Baiu corresponds to the beginning of stage IV in this study, which occurs simultaneously with the onset of the Indian monsoon. The other stages in Ninomiya and Muraki (1986) do not agree with the stages in this study. Also, in order to examine the large-scale situation over East Asia, Matsumoto (1988) divided the period from late summer to autumn into four stages — from stage 1 to stage 4. The ending of stage 1 nearly corresponds to the ending of stage IV, and the beginning of stage 4 also agrees with the beginning of stage I. In addition, Kanno (1988) divided the Bai-u season over East Asia into four stages by considering the positions and the stagnations of frontal zones. The beginning of the late Bai-u nearly coincides with the beginning of stage IV in this study.

As a result, some stages in other studies and in this study nearly agree with each other in spite of the different procedures for dividing the stages. Therefore, the large-scale situations may be closely related to the stratifications of air masses from the Bai-u to the Shurin season. On the contrary, the ending date of the Bai-u season cannot be identified in this study. This implies that the ending of the Bai-u season is mainly affected by atmospheric motions in the tropical area.

Differences of θ and θe between the eastern part of the Eurasian Continent and the Arctic

As seen in Fig. 1, the monthly normal surface air temperatures in January and July indicate the different thermal conditions between the Pc air mass and the A air mass. So, the seasonal variations of thermal differences between the eastern part of the Eurasian Continent and the Arctic in 1985 are investigated.

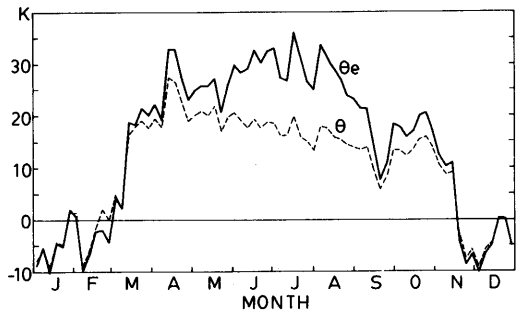

Fig. 5 Difference of the surface potential temperature (θ) and equivalent potential temperature (θe) between the eastern part of the Eurasian Continent and the Arctic in 1985

Figure 5 depicts the temporal variations of surface θ and θe differences between the eastern part of the Eurasian Continent and the Arctic. From late November to mid-February, except for the 6th-7th pentads and the 71st-72nd pentads, the Pc air mass is colder than the A air mass. In late February, around the end of stage I, the θe in the Arctic rises with the increase of water vapor. After early June the θ gradually decreases and, on the contrary, the θe increases. Since this relatively large θe is seen until mid-September, stage IV is characterized as the period in which a large water-vapor difference is formed.

Airmass stratifications in each stage

Figure 6 shows the vertical profiles of temperature and θe in airmass source regions averaged in each stage. The upper limit of the air mass is considered as the height reached by heating and/or cooling from the surface, that is, an inflection point of temperature and θe profiles in the figure.

In stage I, temperature inversions are formed below 850 mb in the Arctic and the eastern part of the Eurasian Continent. Since the stabilities under 700 mb are also large, the upper limits of the A air mass and Pc air mass are regarded as about 700 mb. Compared with the temperature and θe in the Sea of Okhotsk, those in the Bering Sea are higher; warm air advection may be induced by cyclonic activity in the Bering Sea.

In stage II, the stratification, the temperature and θe in the Arctic are nearly the same as those in stage I. Over the Eurasian Continent, temperature and θe largely rise, about 15 degrees at the ground, and the temperature inversion has disappeared. Since a distinct stable layer is formed below 850 mb, the upper limit of the Pc air mass is regarded as this pressure level. The temperature and θe in the Sea of Okhotsk and the Bering Sea show nearly the same profiles.

In stage III, while the temperature inversion below 850 mb becomes weak, the upper limit of the A air mass is still regarded as 700 mb. The vertical profiles of temperature and θe below 700 mb in the eastern part of the Eurasian Continent indicate the least stability of all the airmass source regions by the heating from the surface. The Pc air mass changes its properties after this stage and the upper limit is regarded as 700 mb. In the Sea of Okhotsk stable stratification is seen below 850 mb, so it suggests that the Pm air mass is formed. However, no stable stratification is found in the Bering Sea.

In stage IV, a distinct stable layer is seen below 850 mb in the Arctic, the Sea of Okhotsk, and the Bering Sea. Therefore, the upper limits of the A air mass and Pm air mass are recognized as 850 mb. The Pm air mass in the Sea of Okhotsk is warmer and more stable than that in the Bering Sea. In the eastern part of the Eurasian Continent, the stability under 700 mb is small; in particular, θe_{700}-θe_{850} indicates a minus deviation. Therefore, the upper limit of the Pc air mass in this stage is thought to be 700 mb. Since the vertical profile of potential temperature (dotted line in the figure) does not show unstable stratification, the Pc air mass may be produced by moist convective instability.

In stage V, the stabilities of air masses except for the Eurasian Continent indicate the least value of the year. Especially in the Sea of Okhotsk and the Bering Sea, nearly unstable stratifications are seen under 850 mb. This suggests that sensible heat is supplied from the relatively warm sea surface to the air. On the Eurasian Continent, the

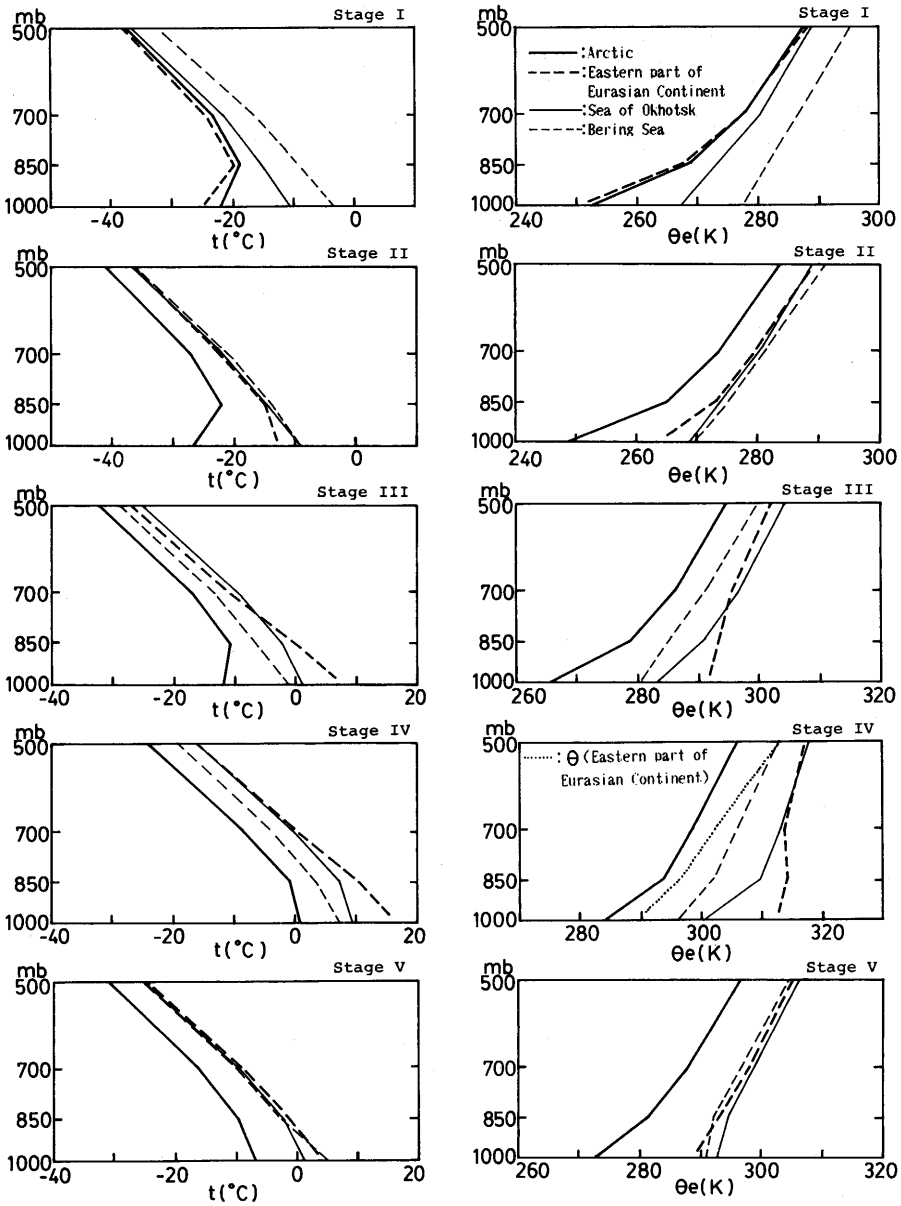

Fig. 6 Vertical profiles of mean temperature and equivalent potential temperature in each stage in 1985

stratification becomes more stable than that in stage III, and the absolute value is nearly the same as those in the Sea of Okhotsk and the Bering Sea. In this stage, the vertical extent of the Pc and A air masses cannot be identified because temperature and θe show nearly linear profiles.

It is worth noting that the stratifications and distributions of air masses in spring

(stage II and III) differ from those in autumn (stage V). These differences may be due to the seasonal variation of sunshine duration and the different heat capacities between the continent and the ocean; however, this hypothesis must be investigated in the future.

5. Seasonal Variations of Airmass Boundaries

The seasonal variations of airmass boundaries are investigated using the time-latitude sections of θe. The airmass boundaries are defined as the large meridional gradient zone of θe. As mentioned in chapter 4, the upper limits of air masses are recognized as 700-850 mb. Since the isobaric surface of 850 mb nearly corresponds to the upper limit and/or inside of the air mass, the analysis for airmass boundary is executed by using the data at the ground.

First, the seasonal variations of the southern boundaries of the A air mass and Pc air mass are investigated using the cross section on the Eurasian Continent. Figure 7 depicts the time-latitude cross-section of five-day mean surface θe averaged from 90°E to 110°E. The meridional gradient of θe ($\nabla\theta e$: K/1000km) is also shown in Fig. 8. The $\nabla\theta e$ is calculated based on the difference between two adjacent mesh data located north and south.

To the south of 35°N, large $\nabla\theta e$ is seen throughout the year. It seems that warm air advection from the Indian Ocean is prevented by the Tibetan Plateau. Also, positive $\nabla\theta e$ is found around 45°N. Since this area corresponds to the Gobi Desert, the air mass may easily be modified. So, this area is defined as the airmass modification zone — the southern boundary of the Pc air mass — and indicated by the broken line in Fig. 8. To the north of 50°N, large $\nabla\theta e$ areas (positive and negative) are clearly seen and they migrate north to south nearly simultaneously with the change of stages. Therefore, the changes of airmass stratification nearly correspond to the migrations of airmass boundaries.

In stage I, a negative $\nabla\theta e$ area is found to the north of 65°N after mid-November. This negative gradient area is produced by the temperature contrast between the A air mass and the Pc air mass (see Fig. 5) and thought to be the boundary between both air masses (broken lines in 70-75°N in Fig. 8). Also after mid-November, large $\nabla\theta e$ is seen about 60°N. Since the Sayan Mountains, Yablonovy Mountains, and Stanovoi Mountains are located in 50-55°N, extremely cold air may be dammed up by these mountains. So, two cold air masses are formed on the Eurasian Continent, and they are distinguished as the Pc_1 (extremely cold) air mass and the Pc_2 (cold) air mass.

In stage II, the negative $\nabla\theta e$ area located along the Arctic coast in stage I nearly disappears and $\nabla\theta e$ becomes large around 60-65°N. Since the A air mass becomes colder than the Pc air mass after stage II, the southern limit of the A air mass is thought to move south, and the large $\nabla\theta e$ area is defined as the airmass boundary between the A air mass and the Pc air mass. The Pc air mass, which is separated into Pc_1 and Pc_2 in stage I, is simplified in this stage. The area in which the Pc_1 air mass is located in stage I is converted into the airmass modification zone.

In stage III, the southern limit of the A air mass discontinuously moves northward

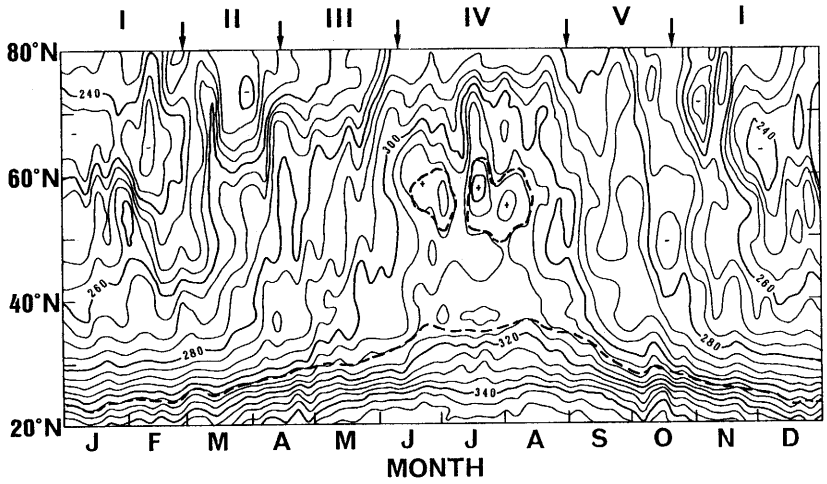

Fig. 7 Time-latitude cross-section of five-day mean surface equivalent potential temperature averaged from 90°E to 110°E in 1985
Arrows and numerals in the upper part of figure indicate the stages. Broken line indicates 8 g/kg of mixing ratio.

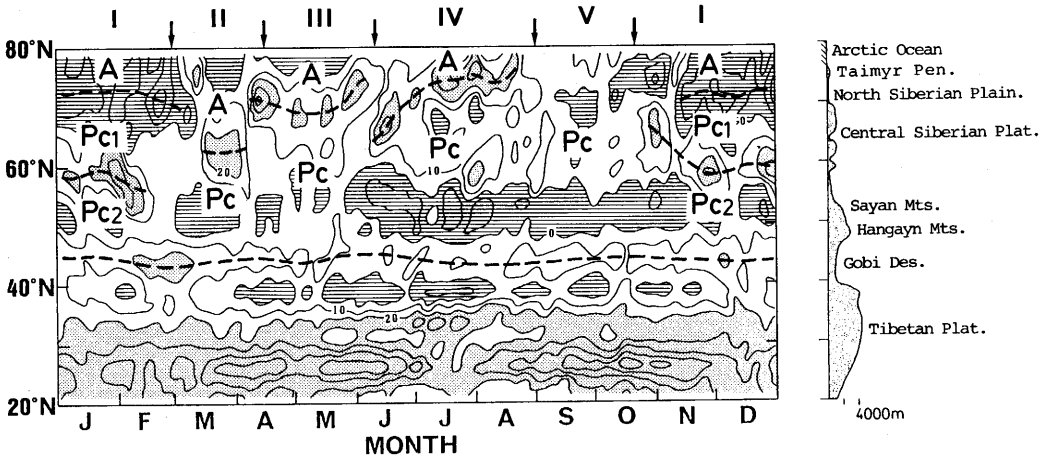

Fig. 8 Time-latitude cross-section of meridional gradient of surface equivalent potential temperature averaged from 90°E to 110°E, and topographic profile along 100°E
Stipplings indicate the area more than 20 K/1000km and hatches indicate the area less than 0 K/1000km. Broken lines indicate the airmass boundaries.

and stagnates in 70-75°N. To the south of this boundary, the Pc air mass spreads to the area around 45°N.

In stage IV, the southern limit of the A air mass tentatively migrates south and north, and then it stagnates around 75°N. Warm and moist air — mixing ratio is over 8 g/Kg — is found in 50-60°N. Since this moist air does not connect with the warm air lying to the south of 35°N, the moisture which characterizes the Pc air mass may not be advected from the south. According to Dr. Kuranoshin Kato (presented in Climatological

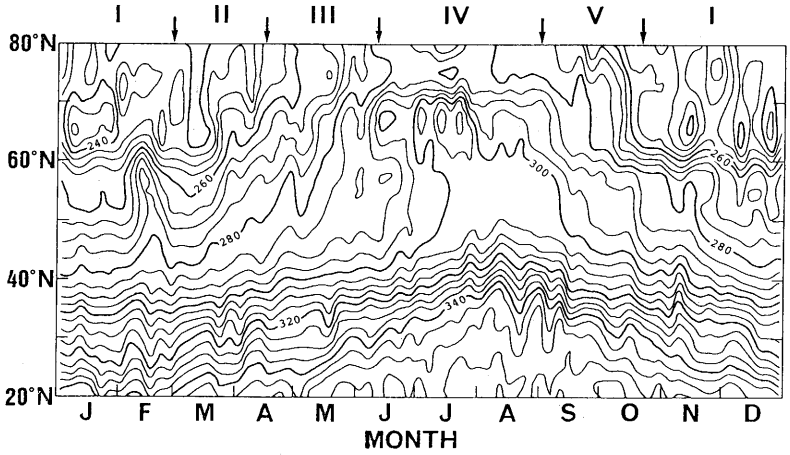

Fig. 9 As in Fig. 7 except for 140°E to 160°E

F9

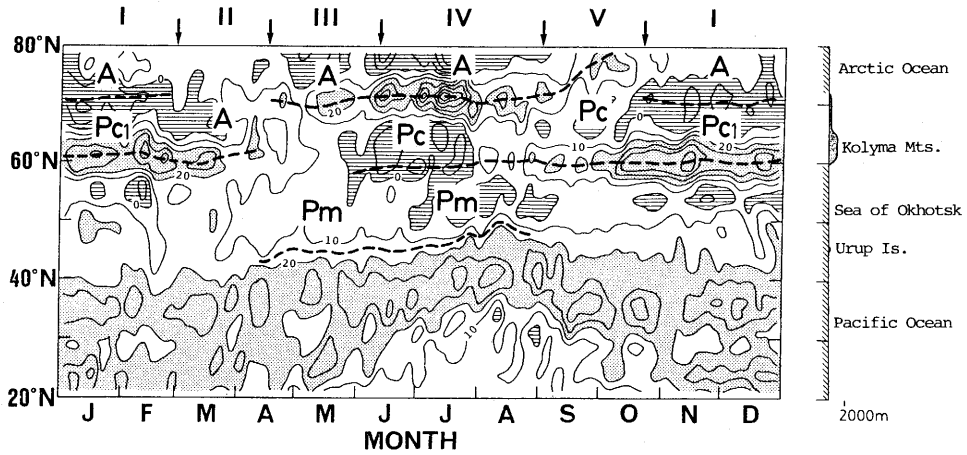

Fig. 10 As in Fig. 8 except for 140°E to 160°E and topographic profile along 150°E

Colloquium on June 6, 1990), the moisture in the air around Lake Baikal is advected from the southeast by the low-pressure field over the desert.

In stage V, the $\nabla\theta e$ lying to the north of 50°N shows the smallest value of the year and so the southern limit of the A air mass cannot be identified. Since the temperature difference between the A airmass and the Pc airmass is large in this stage (see Fig. 5), the airmass boundary may be formed to the north of 80°N.

Next, the period of the Pm air mass formation and the seasonal variations of its boundary are investigated using the time-latitude cross-sections averaged from 140°E to 160°E for the surface θe (Fig. 9) and $\nabla\theta e$ (Fig. 10).

In stage I, the southern limits of the A air mass and the Pc_1 air mass are found around 70°N and 60°N, respectively. Since the $\nabla\theta e$ is large to the south of 50°N, the Pc_2 air mass may be modified with an outbreak over the sea. In stage II, the southern limit of the A air mass moves southward to the area about 60°N.

In stage III, the southern limit of the A air mass discontinuously migrates to around 70°N. The $\nabla\theta e$ becomes small between 45°N and 60°N. Since stable stratification is seen in the low-level layer (see Fig. 6), the Pm air mass may be formed in that small $\nabla\theta e$ area. However, the boundary between the Pc air mass and the Pm air mass is indistinct. The $\nabla\theta e$ to the south of 45°N is large over a vast area. Since the meridional gradient of sea surface temperature in this area is very large with the frontal ground of ocean currents, the modification of the Pm air mass may occur quickly. So, the southern limit of the Pm air mass is defined on the northern edge of the large $\nabla\theta e$ zone — in 40-45° N — shown by the broken line in Fig. 10.

In stage IV, the southern limit of the A air mass is seen about 70°N. Since the Pc air mass is warmer than the Pm air mass until late July (Fig. 9), the northern limit of the Pm air mass is recognized as the negative $\nabla\theta e$ zone about 60°N. The southern limit of the Pm air mass migrates northward to the area in 45-50°N after mid-June; this coincides with the vanishing of the Bai-u front around Japan. To the south of 30-35°N, a maritime tropical air mass is found with small $\nabla\theta e$.

In stage V, the southern limit of the A air mass moves northward to about 75°N. Also, the southern boundary of the Pc air mass is found about 60°N. Since the $\nabla\theta e$ becomes relatively large and the stability is the smallest of the year over the Sea of Okhotsk, a stable Pm air mass is not formed.

6. Frequency of Fronts in Each Stage

The relations between the air masses and frontal zones are investigated by using the cross-section analysis along the meridians. First, in order to examine the seasonal variations of frontal zones, daily positions and frequencies of fronts are investigated on the time-latitude section. The fronts passing through the meridians were picked up and continuous fronts were connected by solid lines. Since the middle latitude area east of 140°E was not analyzed in the synoptic charts used in this study, the longitudinal section along 160°E was not examined. The time-latitude section of the frequency of fronts was comprised of the mean values between 20° longitude. The grids of 5° latitude-longitude mesh size were laid over the daily charts, and the number of fronts passing through or entering each square was tabulated. The total number of fronts in each square was divided by the number of days in each stage and multiplied by one hundred to calculate the percentage frequency of occurrence. The square size was 5° latitude and 10° longitude between 80°N and 85°N. The area north of 85°N was defined as one grid. The types of fronts, such as cold, warm, or occluded fronts, were not differentiated in this procedure.

A modification of the grid in consideration of the latitudinal length was applied by Yoshimura (1967) and Matsumoto (1983). However, a front usually runs from east to west, so the frequencies of fronts in the high latitude area may be overestimated in the modified grid. Therefore, no modification of the grid was applied in this study. Although four meridional sections from 80°E to 140°E are made for the analysis, only the two sections along 100°E and 140°E are shown.

Frequency of fronts along meridians

Frequency of fronts along 100°E

The daily positions of fronts along 100°E are plotted in Fig. 11. The time-latitude sections of frequency of fronts in each stage averaged from 90°E to 110°E are also shown in Fig. 12.

In stage I, the frontal zone is seen around 60°N (Figs. 11 and 12). Since it corresponds to the southern boundary of the Pc_1 air mass (see Fig. 8), this frontal zone is recognized as the polar frontal zone.

In stage II, the frontal zone is seen around 60°N. It is regarded as the Arctic frontal zone. Another concentration of fronts is found in 70-75°N where the frequency is about 15 percent. This suggests that, as can be seen in Fig. 7, relatively warm air is advected to the high-latitude area after early March.

In stage III, the frontal zone is seen around 60°N; this is defined as the Arctic frontal zone. On the other hand, the frequency of about 10 percent is found in 40-45°N in stage III and IV.

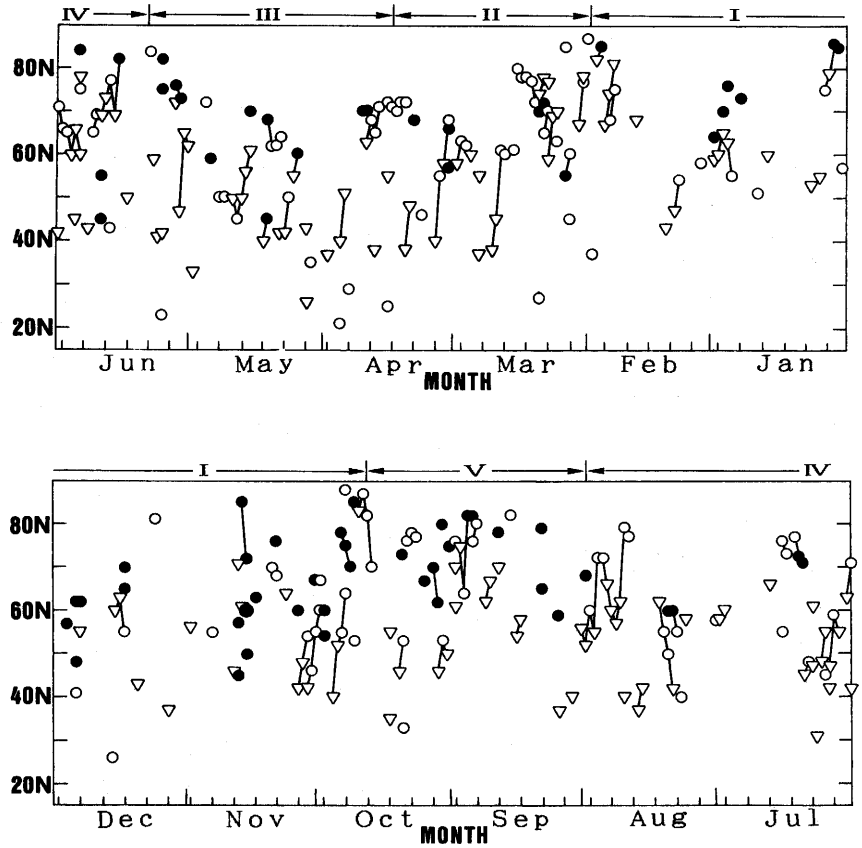

Fig. 11 Daily positions of fronts along 100°E in 1985
▽: cold front, ○: warm front, ●: occluded front
Arrows and numerals in the upper part of the figures indicate the stages.

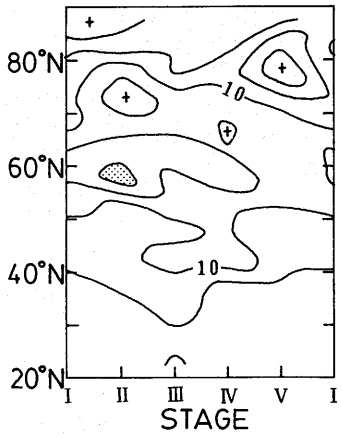

Fig. 12 Time-latitude section of frequency of fronts (%) averaged from 90°E to 110°E
Stipples indicate above 20%, and hatches indicate above 40 %.

In stage IV, the frontal zone is seen in 55-65°N, whereas the fronts seldom appear from late July to early August. This frontal zone is nearly consistent with the southern periphery of the A air mass and the northern periphery of the relatively warm Pc air mass.

In stage V, no distinct frontal zone is seen south of 70°N. On the other hand, a frontal zone whose frequency of occurrence is about 15 percent is seen around 75-80°N. It may be recognized as the Arctic frontal zone, but this is not confirmed in the meridional gradient of θe (Figs. 7 and 8).

Frequency of fronts along 140°E

Along the meridian of 140°E, the fronts frequently appear in the middle and low latitude area, and their seasonal variations are very distinct (Figs. 13 and 14).

In stage I, the fronts frequently appear to the south of 40°N. This frontal zone may be formed around the southern periphery of Pc air mass outbreaks. This is usually called the Pacific polar frontal zone (*e.g.*, Yoshimura, 1967). On the other hand, no frontal zone is found to the north of 40°N.

In stage II, a distinct frontal zone is seen around 30°N. Although fronts appear between 40°N and 70°N, no distinct frontal zone is found.

In stage III, a distinct frontal zone is formed around 30°N (Fig. 14). Another frontal zone is also seen in 45-50°N. According to the daily positions of fronts in Fig. 13, they are formed before mid-May and are concentrated to the south of 40°N. This frontal zone is recognized as the Bai-u frontal zone.

In stage IV, a distinct frontal zone is found around 45-50°N, and this is formed mainly after late July. The other frontal zone located in 30-40°N is defined as the Bai-u frontal zone. It corresponds to the northern periphery of the T air mass (see Figs. 9 and 10).

In stage V, a distinct frontal zone is seen around 30°N. Since the fronts are concentrated around the southern coast of the Japanese Islands from early September to early October, it may be defined as the Shurin frontal zone. No distinct frontal zone is found to the north of 40°N.

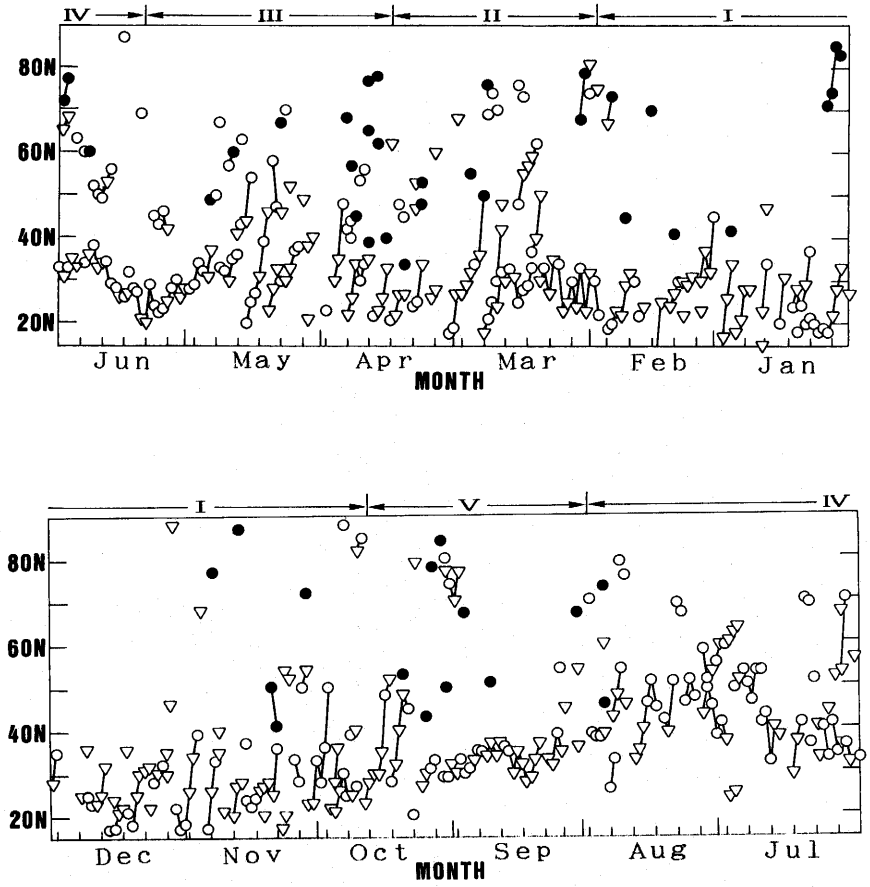

Fig. 13 As in Fig. 11, except for 140°E

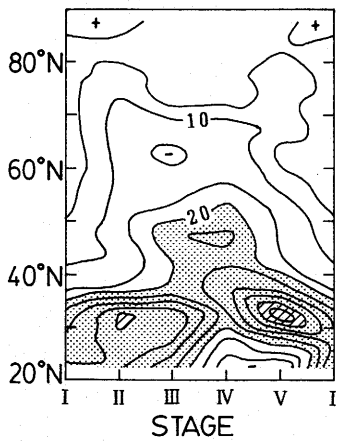

Fig. 14 As in Fig. 12, except for 130°E to 150°E

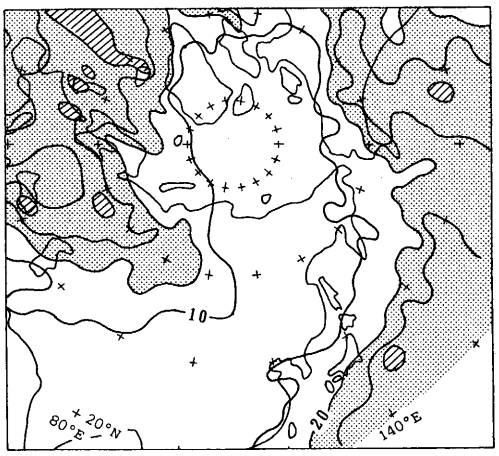

Fig. 15 Percentage frequency of fronts (%) in stage I
Stipples indicate above 20 % and hatches indicate above 40 %.

Frequency distribution of fronts

The frontal zones mentioned above are expressed in the frequency distributions of the fronts in each stage (Figs. 15-19).

Stage I

The percentage frequency of fronts in stage I is shown in Fig. 15. The polar frontal zone can be seen around 60°N west of 100°E. The Pacific polar frontal zone is located in 20-40°N to the east of 130°E. On the other hand, no frontal zone can be found around 60° N between 110°E and 160°E, whereas the southern boundary of the Pc_1 air mass is found in this region (see Fig. 8).

Stage II

The Arctic frontal zone is seen around 60°N west of 130°E (Fig. 16). The Pacific polar frontal zone whose frequency of fronts is greater than that in stage I exists to the south of 40°N east of 120°E.

Stage III

The Arctic frontal zone is located around 60°N west of 100°E (Fig. 17). The area of the Arctic frontal zone becomes rather small in stage III compared with stage II; however, the reason for this reduction is still unsolved. The polar frontal zone is found in 40-50°N east of 120°E. Also, the Pacific polar frontal zone is seen in 30-40°N east of 120°E.

Stage IV

The Arctic frontal zone is seen around 60°N west of 130°E, whereas a few fronts appear east of 130°E (Fig. 18). The polar frontal zone can be seen from 60°N and 100° E to 40°N and 180°. The Bai-u frontal zone exists around 40°N between 140°E and 160° E.

Stage V

The Arctic frontal zone can be found around 80°N and 80°E (Fig. 19). The polar frontal zone exists around 60°N west of 120°E. The Pacific polar frontal zone (Shurin frontal zone) where the frequency of fronts is the largest of all stages is located in 30-35° N between 130°E and 160°E.

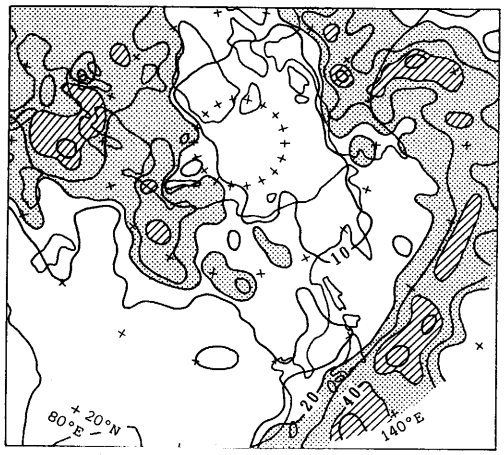

Fig. 16 As in Fig. 15, except for stage II

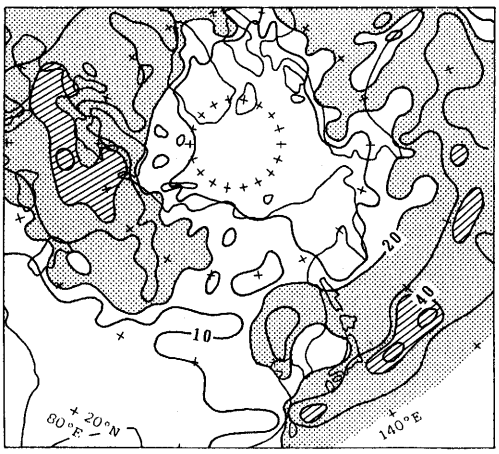

Fig. 17 As in Fig. 15, except for stage III

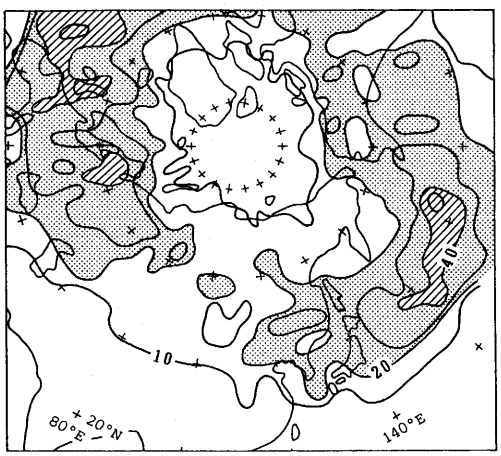

Fig. 18 As in Fig. 15, except for stage IV

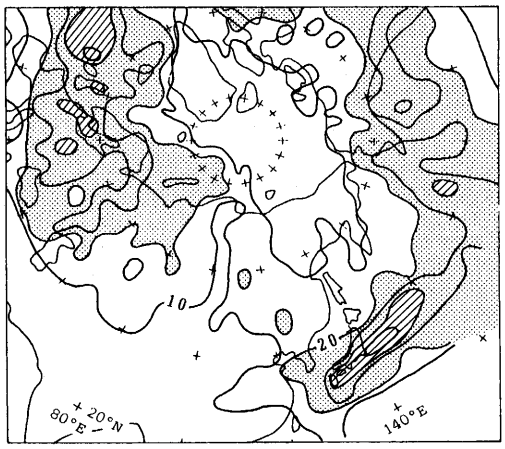

Fig. 19 As in Fig. 15, except for stage V

7. Vertical Structures of Air Masses and Fronts

The vertical structures of fronts and air masses are investigated based on the cross sections along the meridians in each stage. The upper air observation stations located in the areas of 20° longitude south of 60°N, 60° longitude between 60°N and 70°N, and 120° longitude between 70°N and 80°N were utilized for this analysis. In the following, the important examples are described in each stage.

Stage I

The case for February 2, 1985 is selected as an example for stage I. The surface θe and fronts are illustrated in Fig. 20. The Pc_2 air mass exists north of 40°N and also the Pc_1 air mass is located to the north of 60°N in the eastern part of the Eurasian Continent. The polar front is found around 60°N and 80°E, and the Pacific polar front lies from south of Taiwan to south of Kamchatka Peninsula.

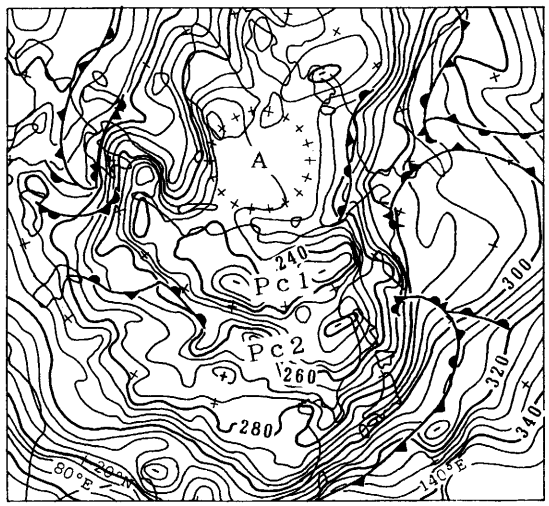

Fig. 20 Surface equivalent potential temperature (K) and fronts at 00GMT February 2, 1985 Names of air masses are shown in figure.

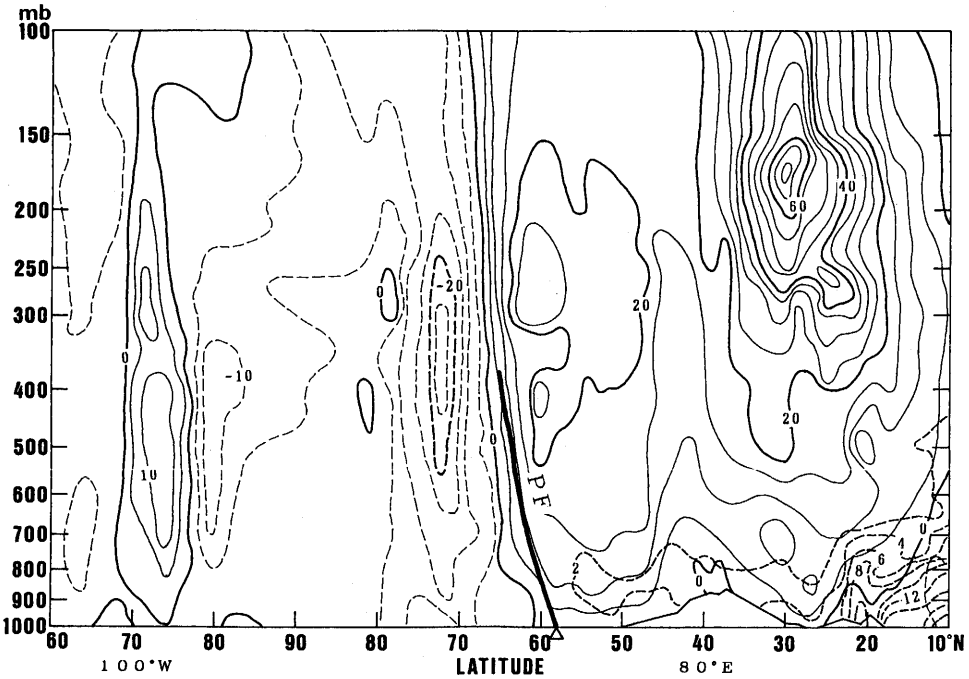

Fig. 21 Vertical cross-section of u-component (m/s, in solid and broken lines) and specific humidity (g/kg, thick broken lines) along 80°E to 100°W at 00GMT February 2, 1985 Names of air masses and frontal zones are shown in figure.

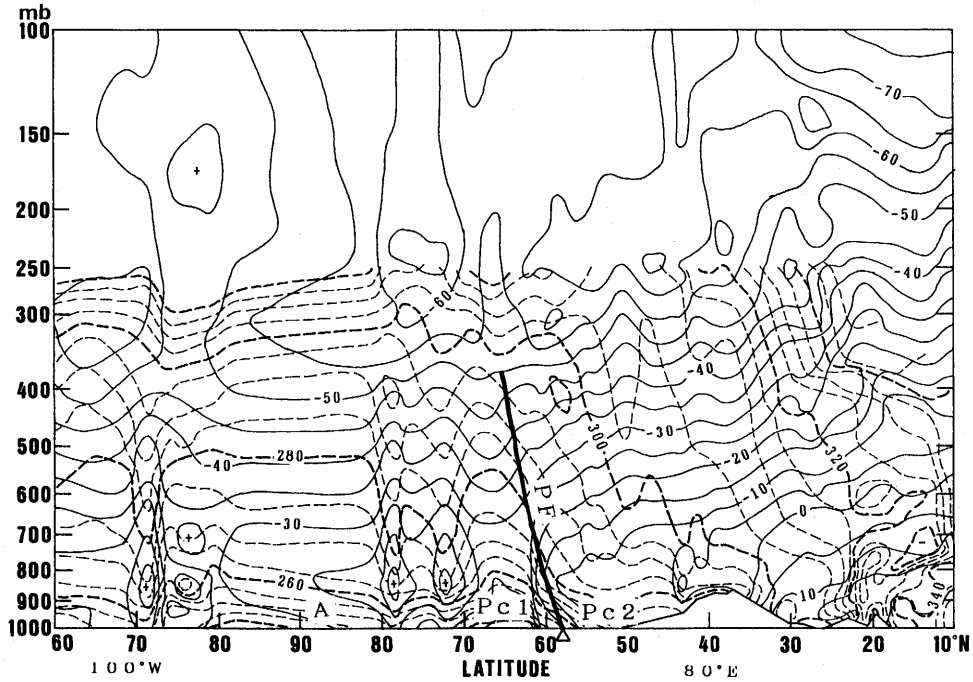

Fig. 22 Vertical cross-section of temperature (°C, solid lines) and equivalent potential temperature (K, broken lines) along 80°E to 100°W at 00GMT February 2, 1985

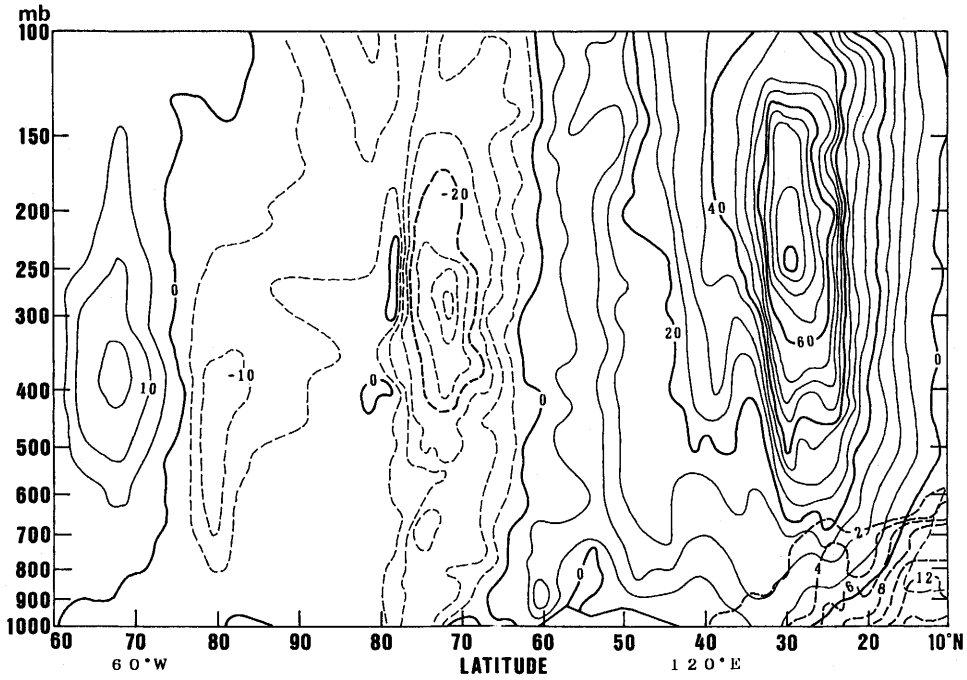

Fig. 23 As in Fig. 21, except for 120°E to 60°W

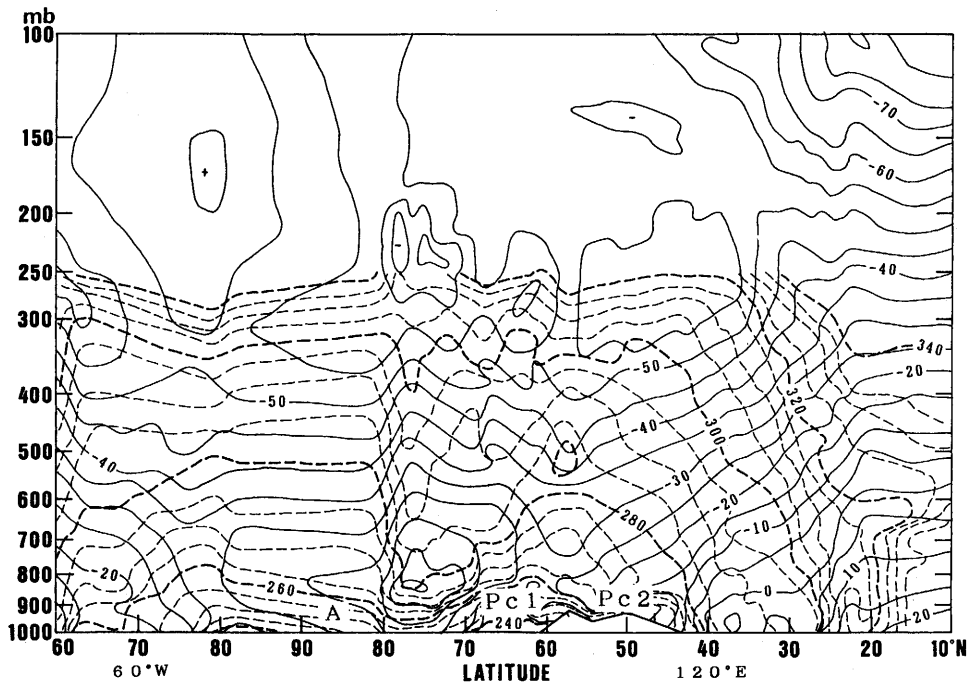

Fig. 24 As in Fig. 22, except for 120°E to 60°W

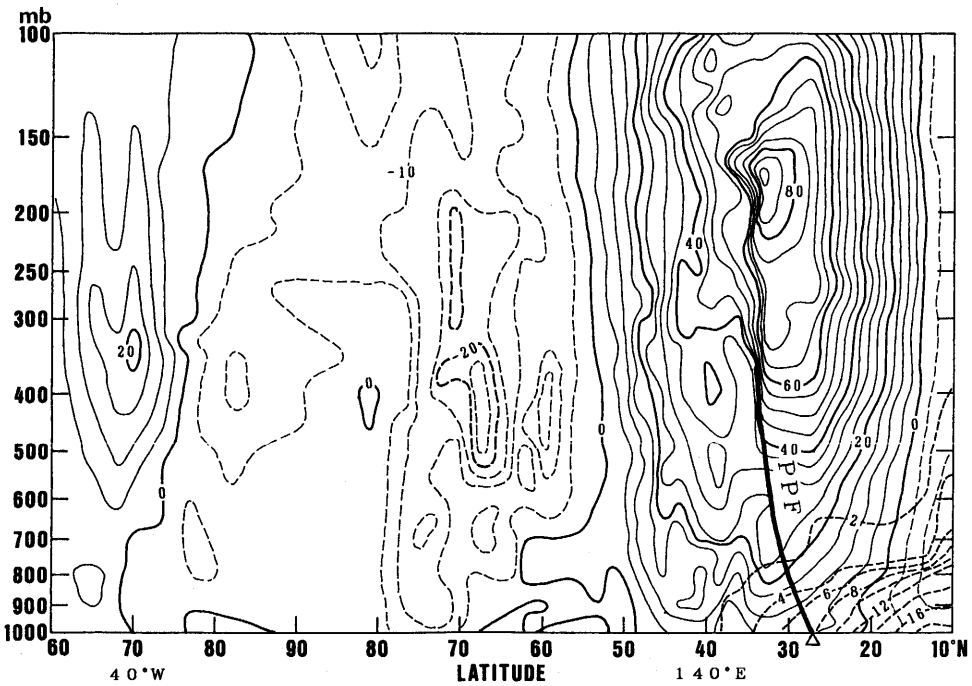

Fig. 25 As in Fig. 21, except for 140°E to 40°W

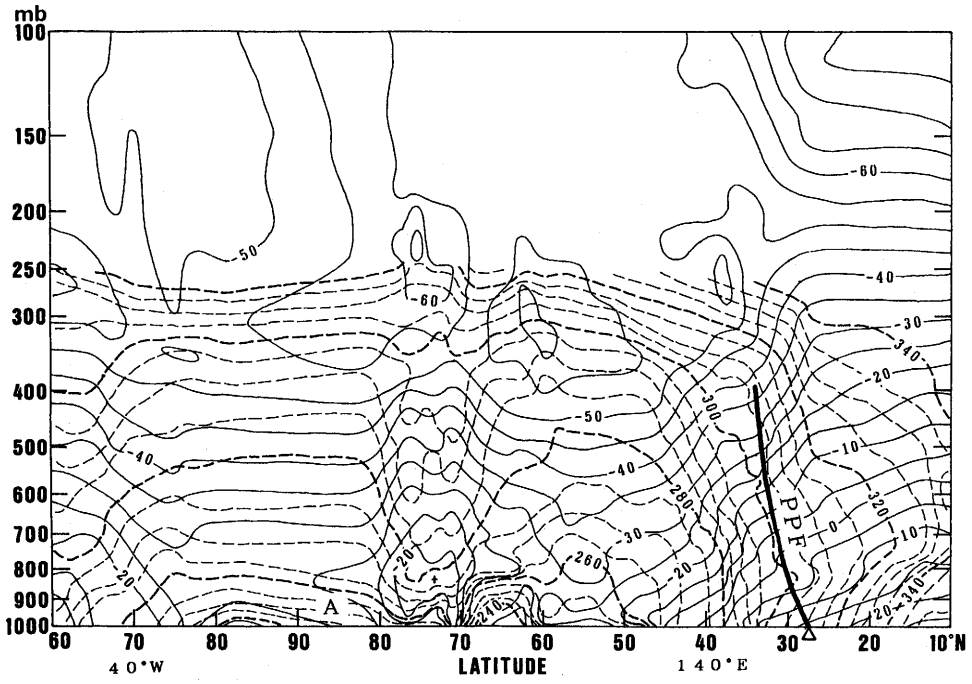

Fig. 26 As in Fig. 22, except for 140°E to 40°W

The vertical cross-sections of u-component, specific humidity, temperature, and θe along 80°E to 100°W are shown in Figs. 21 and 22. The polar front (PF in the figure) is connected with the strong westerly wind located in 200-300 mb (Fig. 21). Although another jet stream is seen around 30°N, no front is analyzed with it. The polar front is formed at the southern periphery of the very stable Pc_1 air mass, and the meridional gradients of temperature and θe around this front are very large (Fig. 22). In addition, the specific humidity is very small over the continent.

The vertical structures of the A air mass, Pc_1 and Pc_2 air masses along 120°E to 60°W are illustrated in Figs. 23 and 24. In stage I, no frontal zone is found along this longitudinal section and an axis of strong westerly wind is not formed to the north of 40°N (Fig. 23). The jet stream is present in 25-30°N, although a front is not associated with it. The A air mass lies to the north of 70°N and a temperature inversion is seen below 800 mb (Fig. 24). The Pc_1 and Pc_2 air masses exist between 40°N and 70°N and a distinct temperature inversion can be seen below 800 mb. The center of the Pc_1 air mass is found between 60°N and 70°N, and the Yablonovy Mountains seems to dam up this air mass. On the other hand, no stable stratification in the lower layer is seen to the south of 40°N; therefore, the Pc_2 air mass may be modified over the ocean.

The vertical structure of the Pacific polar front (PPF) located at the southern coast of Japan is shown in Figs. 25 and 26. This front is connected with a jet stream whose wind speed is greater than 80 m/s (Fig. 25). No other axis of strong westerly wind is found in the middle and high latitudes along 140°E. The specific humidity is relatively large to the south of the Pacific polar front. The meridional gradients of temperature and θe are large to the south of 40°N; besides, the meridional gradients are not very large and relatively unstable stratification is seen between 40°N and 60°N (Fig. 26). Since the air located to the south of 60°N may be recognized as the modified Pc_1 and/or Pc_2 air masses, the Pacific polar front is formed around the southern periphery of Pc air mass outbreaks.

Stage II

The case for March 31, 1985 is selected as an example for stage II (Fig. 27). The Arctic air mass exists over the high latitude area and the Arctic front is formed around the North Siberian Plain. Since the meridional gradient of θe between 40°N and 60°N over the Eurasian Continent is small, it is confirmed that the Pc air mass is located in this region. The Pacific polar front is located from the southern coast of Japan to south of Kamchatka Peninsula.

The vertical cross-sections along 100°E to 80°W are shown in Figs. 28 and 29. The Arctic front (AF) is connected with a strong westerly wind whose elevation is relatively low (Fig. 28). While another strong westerly wind is seen in 30-40°N, the front is not analyzed. The specific humidity is small to the north of 30°N. The top of a temperature inversion is seen around 850 mb in the A air mass (Fig. 29). The Arctic front is formed at the southern periphery of the A air mass and large meridional gradients of temperature and θe can be found around this front. Compared with the stratification of the Pc_1 air mass in stage I, the stability of the Pc air mass is not very large in this stage.

The vertical structure of the Pacific polar front located at the southern coast of Japan is shown in Figs. 30 and 31. This front is connected with a jet stream whose wind

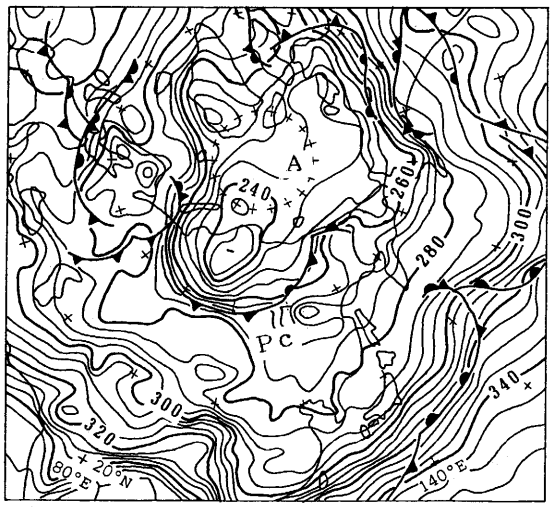

Fig. 27 As in Fig. 20, except for March 31, 1985

speed is greater than 60 m/s (Fig. 30). No other axis of strong westerly wind is found distinctly in the middle and high latitudes. While the Arctic front is analyzed around 70° N, it is not clearly seen along this longitudinal section. The specific humidity is relatively large to the south of the Pacific polar front. The meridional gradient of θe is very large around the Pacific polar front (Fig. 31). The meridional gradient and the stability are small to the north of this front.

Stage III

The case for May 11, 1985 is selected for analysis (Fig. 32). Small meridional gradient areas are found around the Arctic, the eastern part of the Eurasian Continent, and from the Sea of Okhotsk to the Bering Sea, and the air masses are formed in these areas. The Arctic front is formed around the southern periphery of the A air mass on the Eurasian Continent. The polar front is seen in 40-45°N from 100°E to 170°E and the Pacific polar front is located from the southern coast of Japan to south of the Bering Sea.

The vertical cross-sections along 100°E to 80°W are shown in Figs. 33 and 34. The Arctic front is connected with the strong westerly wind located in 55-65°N (Fig. 33). The polar front is also accompanied by a strong westerly wind. The specific humidity is small to the north of 30°N. The Arctic front is formed at the southern periphery of the A air mass, whereas the meridional gradient of temperature and θe around this front are not very large (Fig. 34). The polar front is formed at the southern periphery of the Pc air mass, whose stratification is relatively unstable below 700 mb. The meridional gradient of θe is very large around the polar front.

The vertical cross-sections along 140°E are shown in Figs. 35 and 36. The polar front located in 47°N is not connected with a strong westerly wind, and the specific humidity to the south of it is also relatively small (about 4 g/kg). On the other hand, the Pacific polar front is accompanied by a strong westerly wind, and the specific humidity to the south of it is relatively large (more than 10 g/kg). The Pm air mass can be seen between 50°N and 60°N (Fig. 36). The polar front is formed at the southern periphery

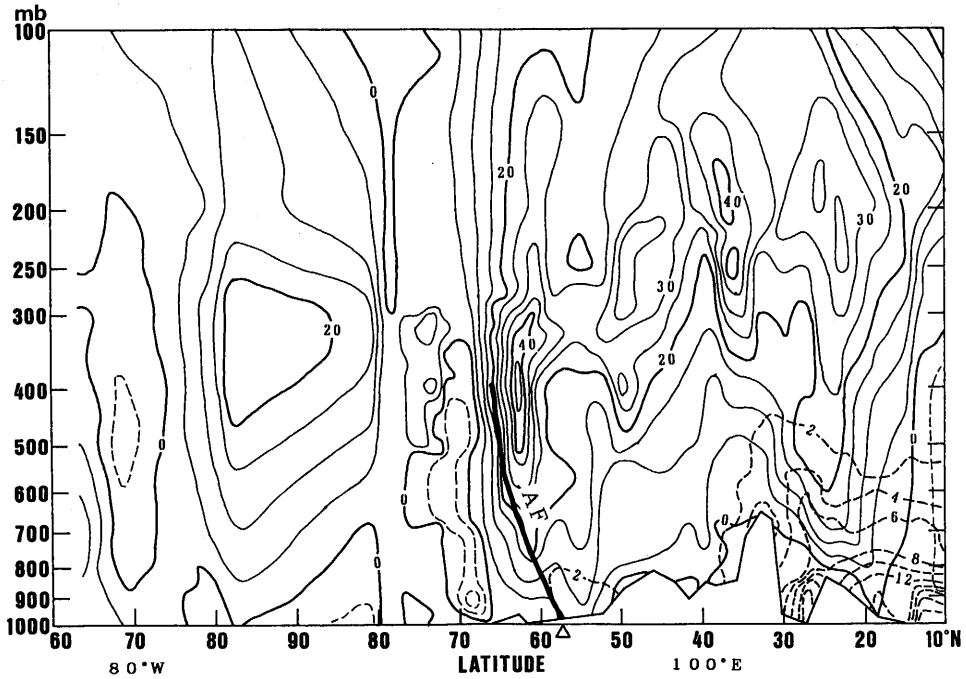

Fig. 28 As in Fig. 21, except for 100°E to 80°W on March 31

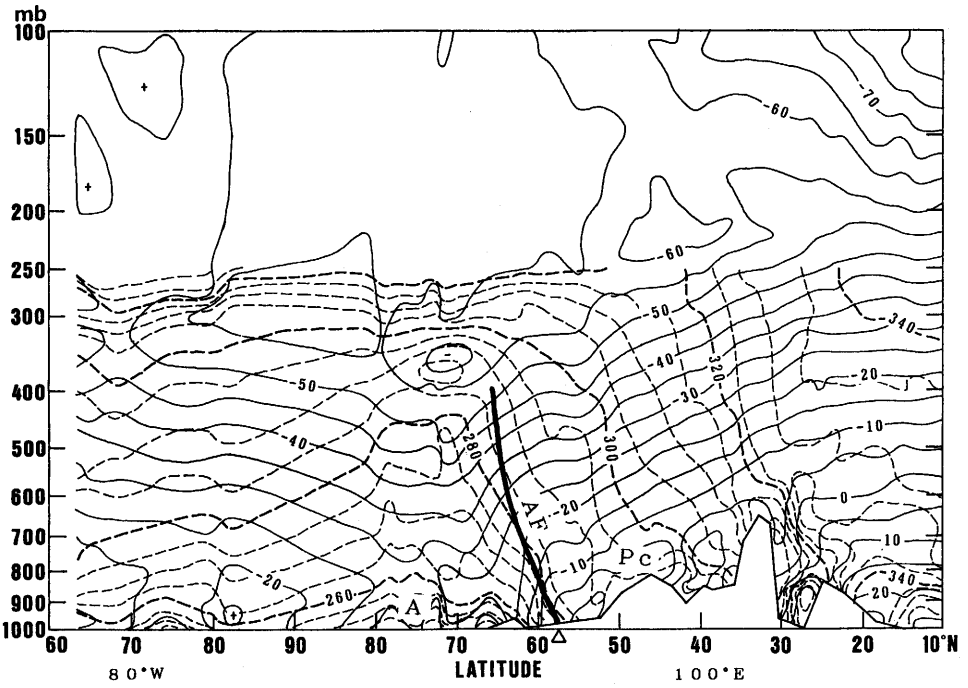

Fig. 29 As in Fig. 22, except for 100°E to 80°W on March 31

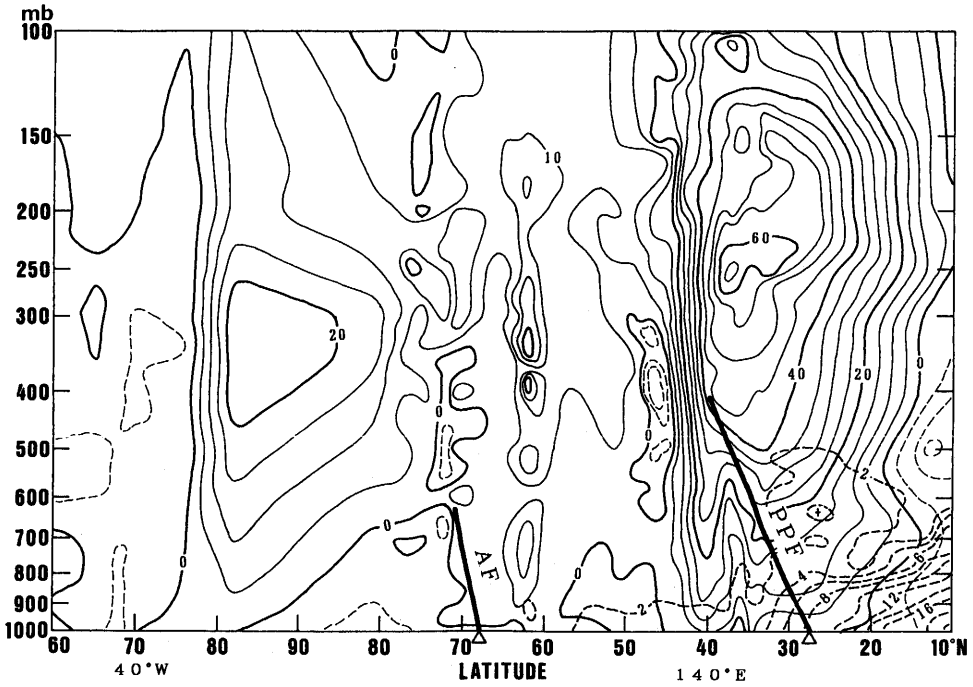

Fig. 30 As in Fig. 21, except for 140°E to 40°W on March 31

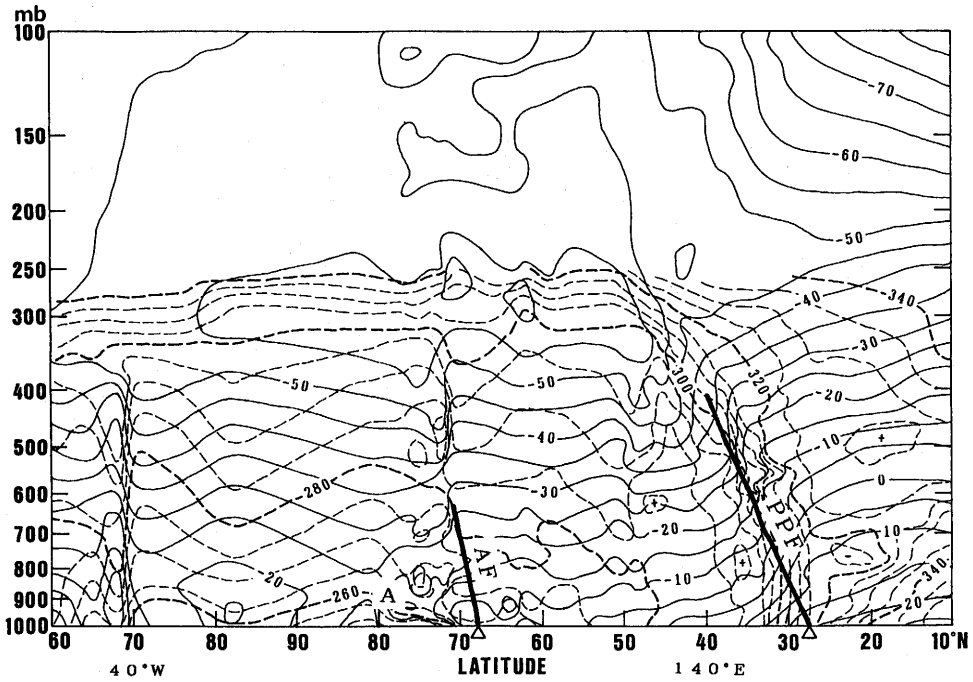

Fig. 31 As in Fig. 22, except for 140°E to 40°W on March 31

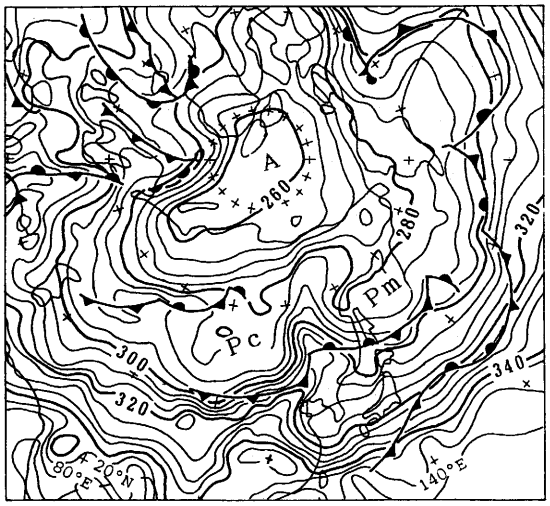

Fig. 32 As in Fig. 20, except for May 11

of the Pm air mass. On the other hand, the meridional gradient of θe around the Pacific polar front is not very large. The hot and humid air — T air mass — is seen to the south of the Pacific polar front.

Stage IV

The cases for July 30 and August 6, 1985 are selected in stage IV. The A air mass and Pm air mass are clearly seen, whereas the meridional gradient in the eastern part of the Eurasian Continent is relatively large (Fig. 37). The Arctic front is analyzed around 60°N on the Eurasian Continent.

On the vertical cross-section along 100°E and 80°W, the Arctic front is connected with the axis of westerly wind whose elevation is 400-500 mb (Fig. 38). The specific humidity is large in the entire low-level layer to the south of 70°N. Strong westerly wind is seen in the upper troposphere around 40°N, whereas no front is connected with it. The Arctic front is formed around the southern periphery of the A air mass (Fig. 39). Also, a large meridional gradient of θe can be seen around 70°N. The stratification of the Pc air mass is generally unstable in the middle- and low-level layers.

The surface θe and fronts on August 6 are illustrated in Fig. 40. The polar front is seen around the southern periphery of the Pm air mass.

On the vertical cross-section along 140°E, the polar front is connected with the strong westerly wind (Fig. 41). The amount of moisture in the air is large to the south of this front. The polar front is recognized as the large meridional gradient zone of θe, whereas the temperature gradient is not very large (Fig. 42). While the meridional gradient of θe is small to the north of this front, no distinct stable stratification can be found. Since this longitudinal section is located at the western periphery of a relatively weak Pm air mass in this stage, the stable air mass is not analyzed. Although no cross section can be made to the east of this transection because of the scarcity of data, a front may be formed at the southern periphery of the Pm air mass. The southern boundary of the A air mass is found distinctly around 70°N, whereas the Arctic front is not analyzed.

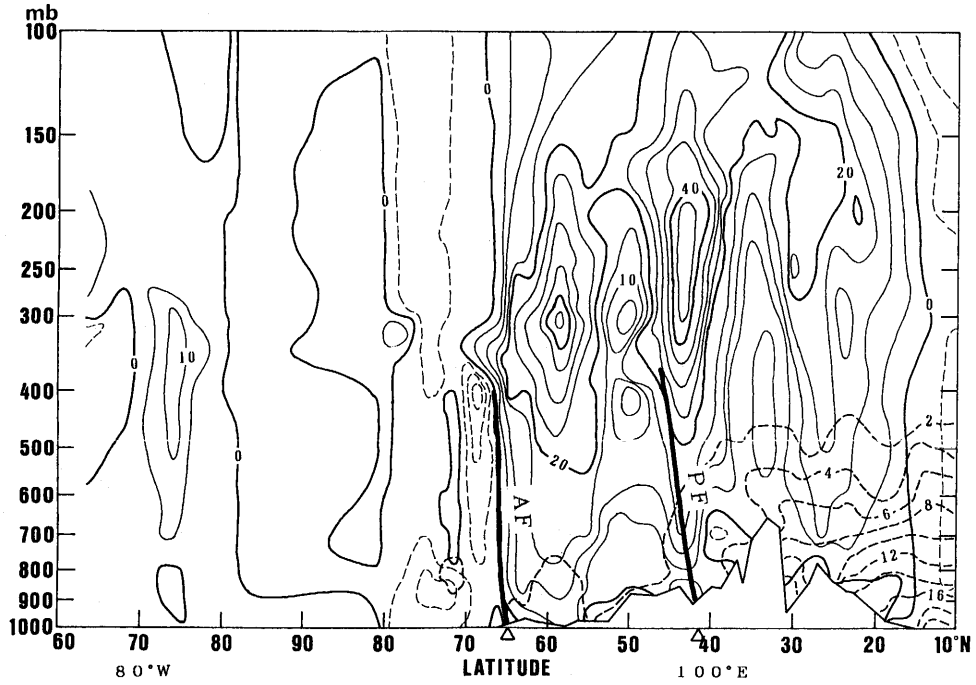

Fig. 33 As in Fig. 21, except for 100°E to 80°W on May 11

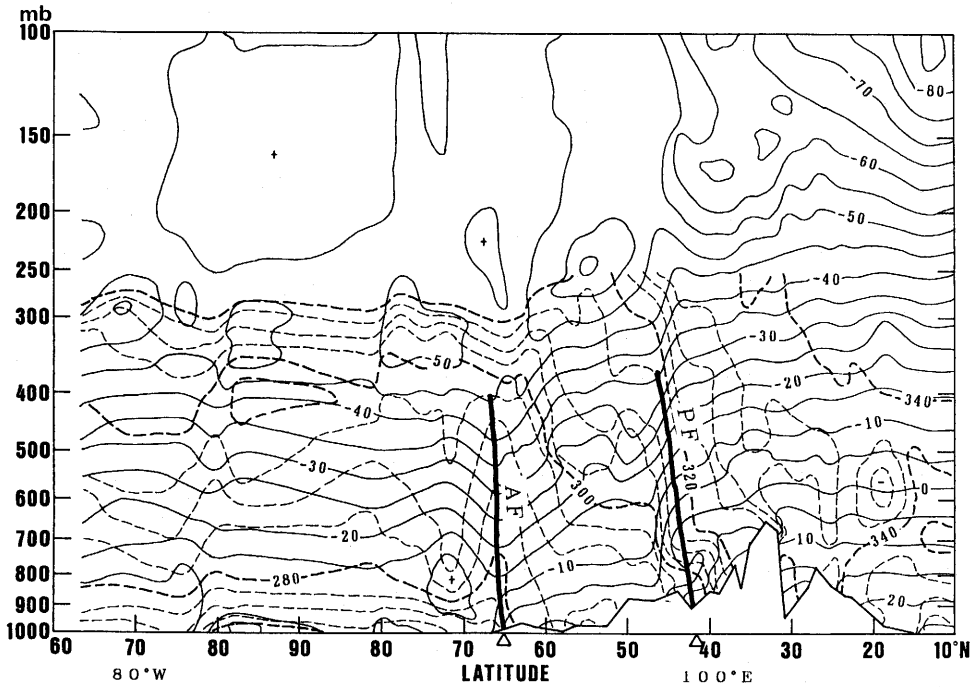

Fig. 34 As in Fig. 22, except for 100°E to 80°W on May 11

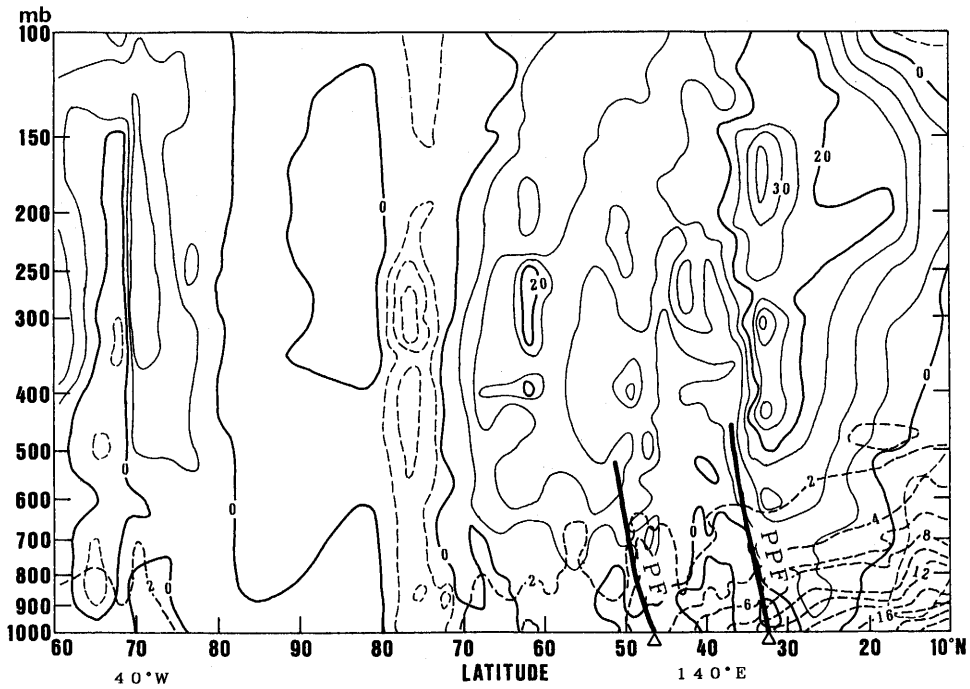

Fig. 35 As in Fig. 21, except for 140°E to 40°W on May 11

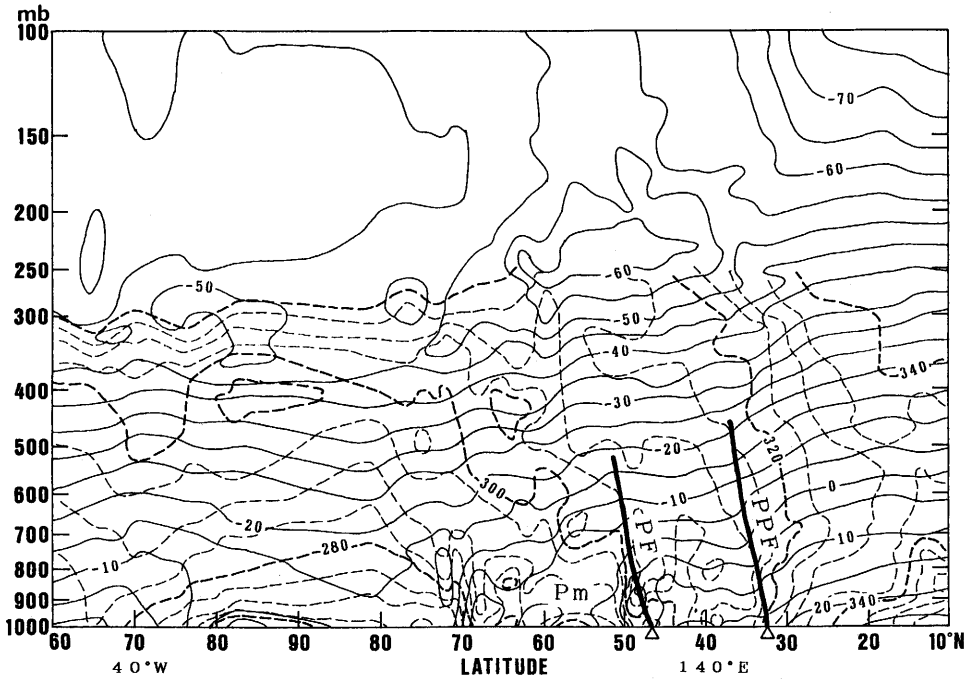

Fig. 36 As in Fig. 22, except for 140°E to 40°W on May 11

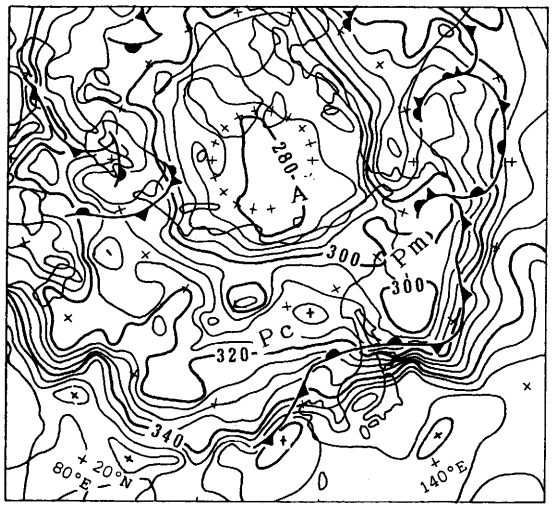

Fig. 37 As in Fig. 20, except for July 30

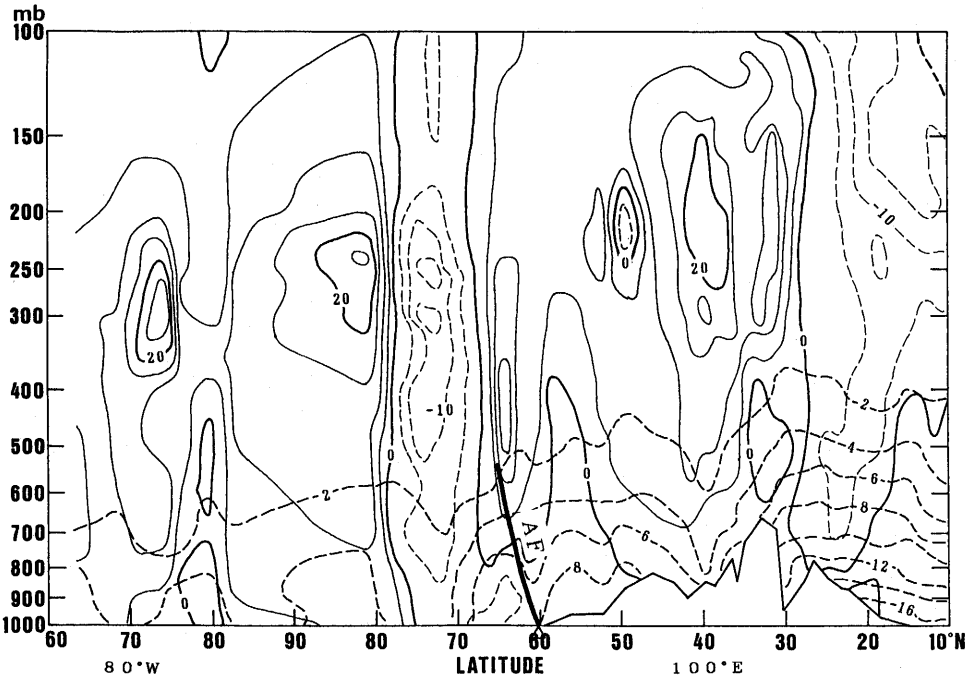

Fig. 38 As in Fig. 21, except for 100°E to 80°W on July 30

Stage V

The case for September 15, 1985 is selected for the analysis (Fig. 43). The meridional gradient of θe is small in the Arctic and over the Eurasian Continent, whereas it is large in the Sea of Okhotsk and the Bering Sea. The Arctic front is located at northern

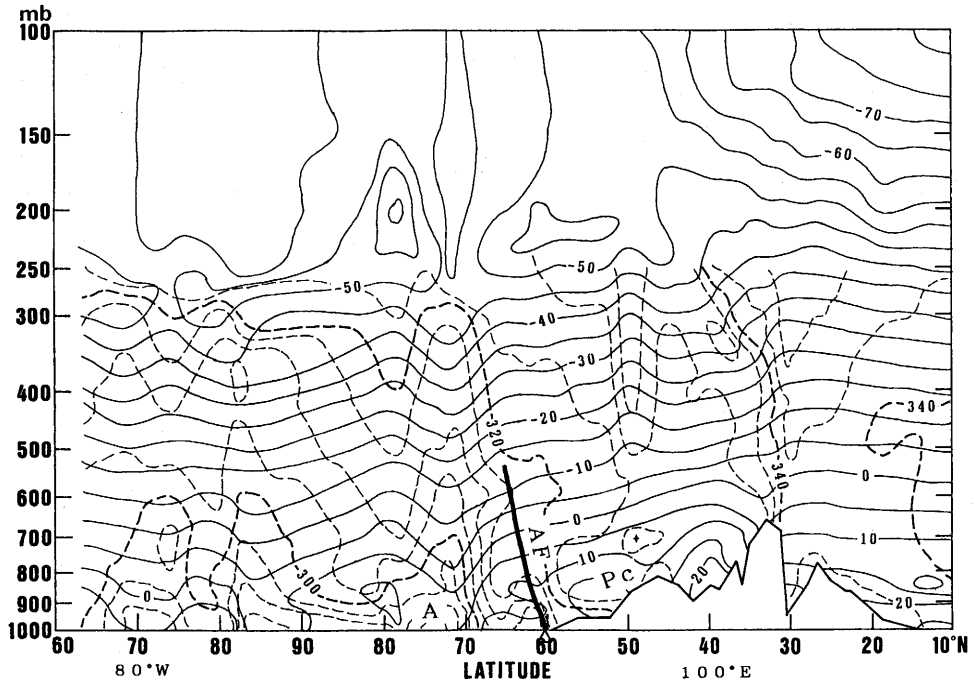

Fig. 39 As in Fig. 22, except for 100°E to 80°W on July 30

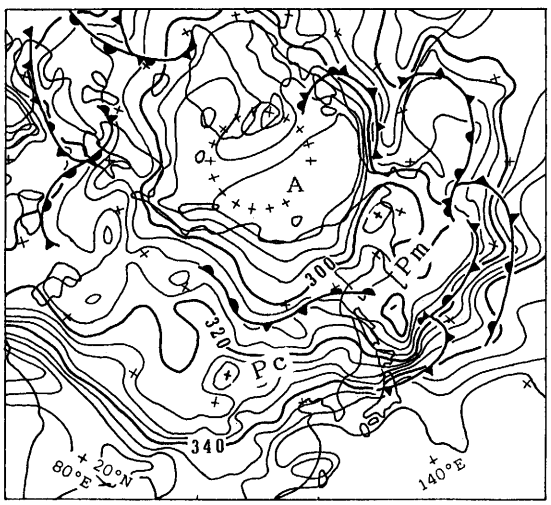

Fig. 40 As in Fig. 20, except for August 6

Novaya Zemlya, and the polar front is found on the Eurasian Continent. The Pacific polar front is seen from the China Continent to the south of the Bering Sea.

The vertical cross-sections along 80°E to 100°W are shown in Figs. 44 and 45. The Arctic front and the polar front are connected to the strong westerly wind. (Fig. 44).

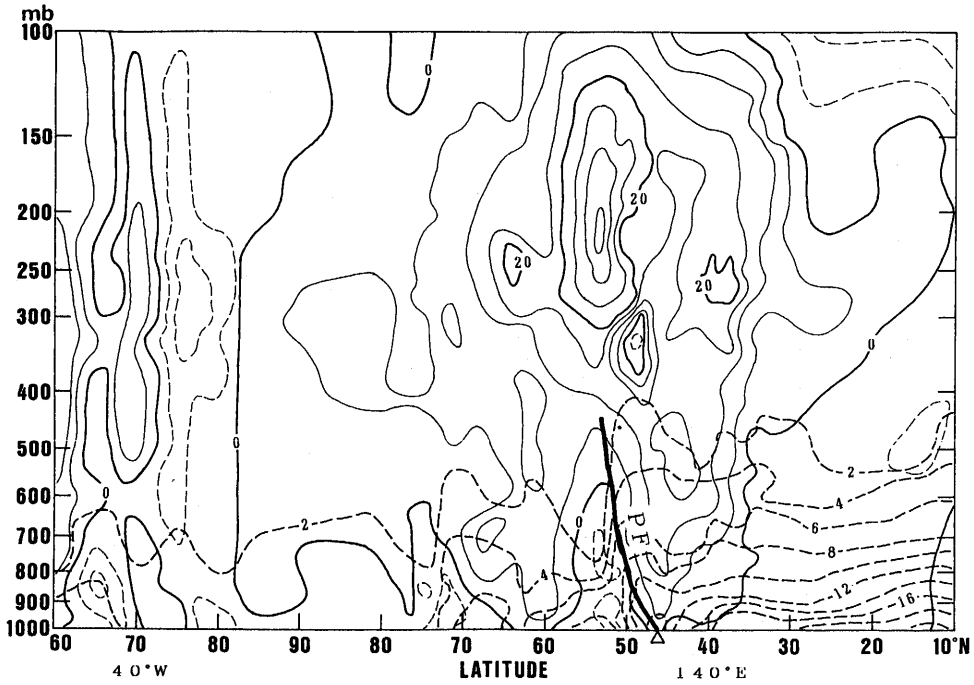

Fig. 41 As in Fig. 21, except for 140°E to 40°W on August 6

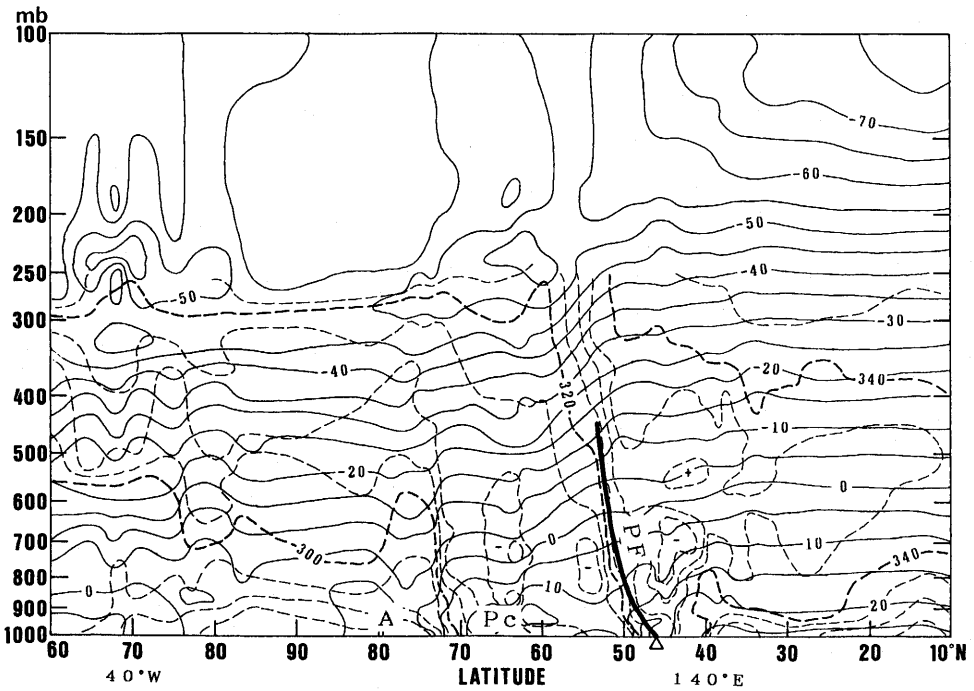

Fig. 42 As in Fig. 22, except for 140°E to 40°W on August 6

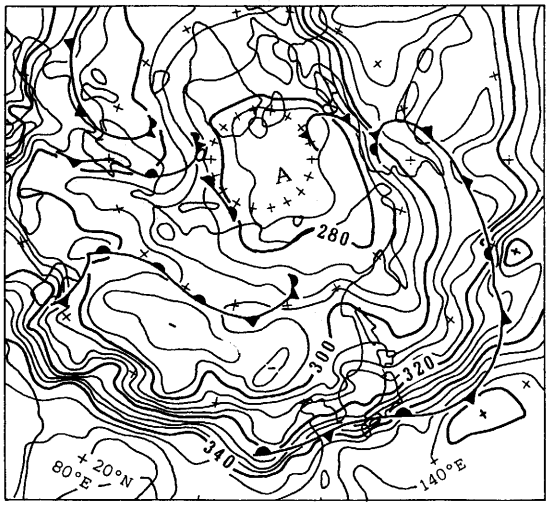

Fig. 43 As in Fig. 20, except for September 15

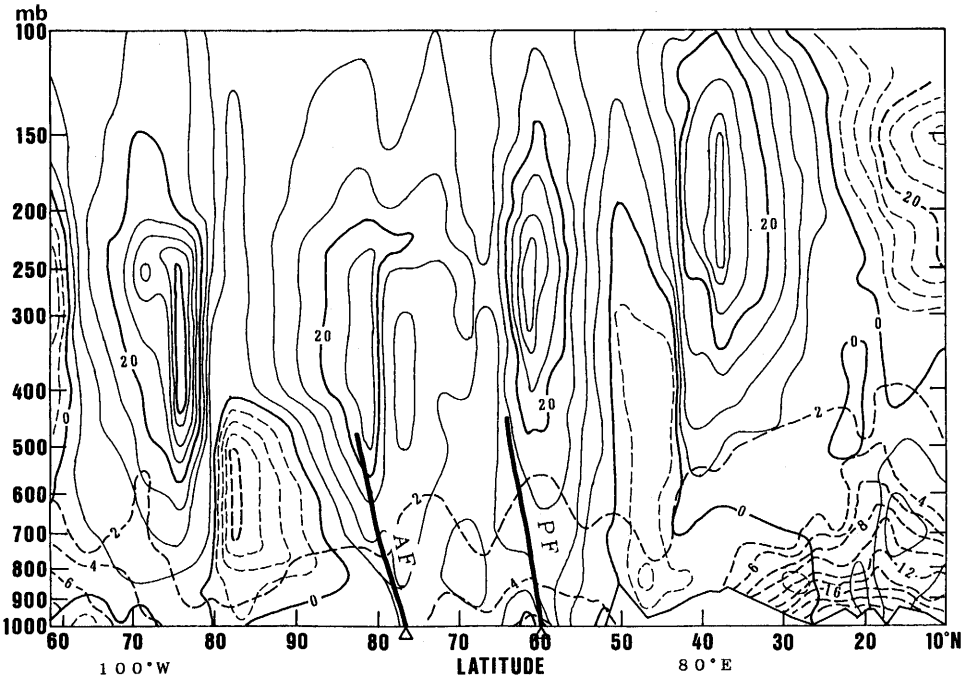

Fig. 44 As in Fig. 21, except for 80°E to 100°W on September 15

While another strong westerly wind can be seen around 30-45°N, no front is associated with it. The specific humidity is small to the north of 40°N. The meridional gradient of θe is small around the Arctic front and the polar front (Fig. 45). In general, the meridional gradient of θe is not large and the stratification is relatively stable to the

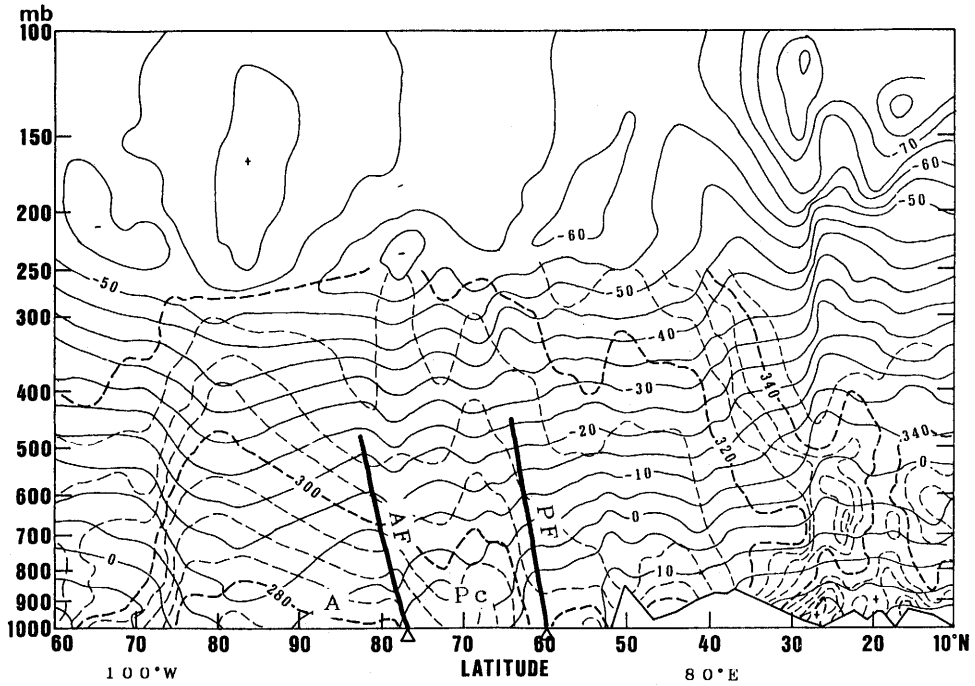

Fig. 45 As in Fig. 22, except for 80°E to 100°W on September 15

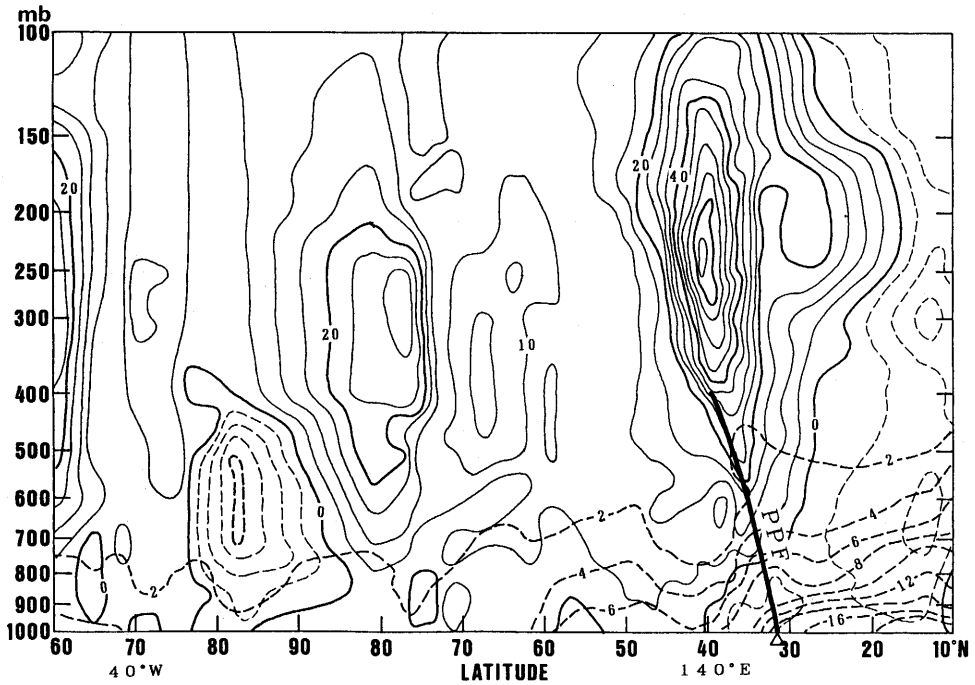

Fig. 46 As in Fig. 21, except for 140°E to 40°W on September 15

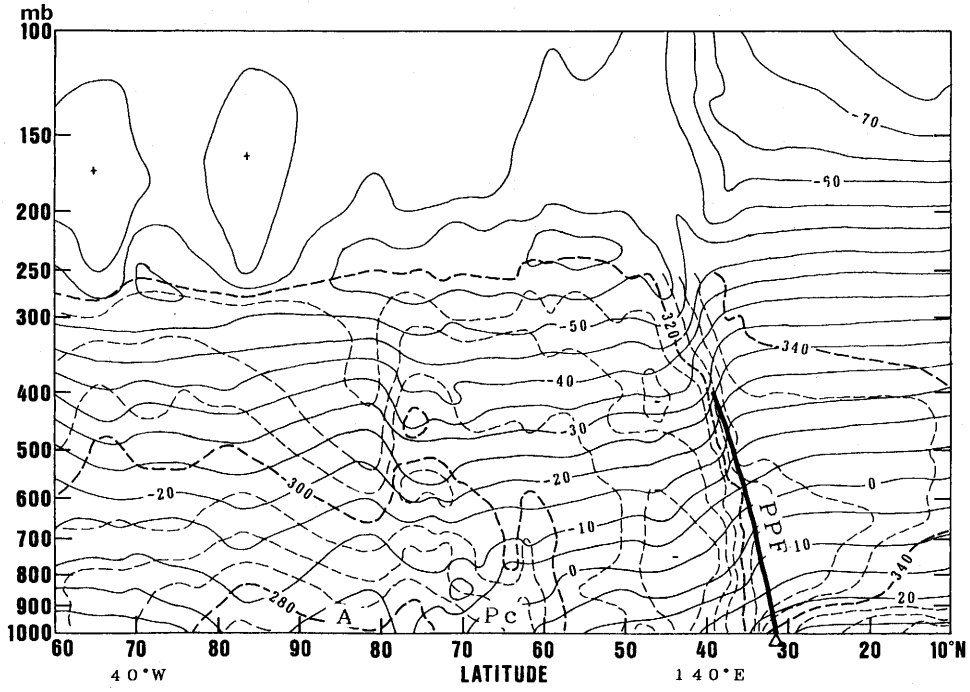

Fig. 47 As in Fig. 22, except for 140°E to 40°W on September 15

north of 35°N.

The vertical cross-sections along 140°E are shown in Figs. 46 and 47. The Pacific polar front and θe are connected with the strong westerly wind, and the meridional gradient of specific humidity and θe are large around this front. The southern boundary of the Pc air mass is seen around 60°N. Since the θe gradient is small to the north of 60° N, the southern boundary of the A air mass cannot be identified.

Comparisons between the frontal zones in this study and other studies

The frontal zones in this study are defined by use of the synoptic charts for 1985. So, in order to consider the peculiarities of the year 1985 and the synoptic charts, the comparison of distribution of frontal zones in this study with those in other studies is necessary.

Schumann and van Rooy (1951) showed the percentage frequency of fronts in winter from December to February, and in summer from June to August, although the area west of 120°E was not investigated. According to their study, no frontal zone was found to the north of 60°N and east of 120°E in winter or summer. On the contrary, a relatively weak frontal zone is seen around 60°N in summer in this study.

Reed (1960) showed the polar frontal zone in 50-60°N west of 120°E in winter from December to February. This is in good agreement with the position of the polar frontal zone in stage I. He also showed the Eurasian polar frontal zone around 40°N west of 100° E. While this frontal zone corresponds to the southern boundary of the Pc air mass, it

cannot be found in this study. The positions of the Pacific polar frontal zone in Reed's study and in this paper are well correlated. In summer from June to August, the Siberian-Canadian Arctic frontal zone represented by Reed (1960) is in good agreement with the Arctic frontal zone in stage IV. The Eurasian polar frontal zone and the Pacific polar frontal zone also nearly correspond to those in this study.

Yoshimura (1967) showed monthly positions of frontal zones in the Northern Hemisphere. The Mediterranean branch of the Eurasian polar frontal zone was located around 40°N west of 100°E in December and February, which was also shown by Reed (1960). However, this frontal zone is not analyzed in this paper. So, it seems that the front is hardly analyzed around 40°N over the continent on the synoptic charts used in this study, and/or no front existed around that area in 1985. In any case, the frontal zone may be present around the southern periphery of the Pc_2 air mass around 40°N in stage I, although it is not analyzed in this work. A distinct Siberian-Canadian Arctic frontal zone exists with a percentage frequency more than 50 percent from June to September in Yoshimura (1967); however, the percentage frequency of the Arctic frontal zone is 10-20 percent in this study in stage IV. It is probable that the modification for the grid in his study produces the surplus percentage frequency. On the other hand, the polar frontal zone in the Eurasian Continent defined in this paper does not appear in Yoshimura (1967). Since that frontal zone was also analyzed in Reed (1960), the synoptic charts used in Yoshimura (1967) may not indicate a front in that region.

Matsumoto (1983) showed the winter locations of the Arctic frontal zone, which are in good agreement with the polar frontal zone in stage I.

8. Conclusions

The seasonal variations of stratification and distribution of air masses in the Arctic and the middle and high latitudes in the eastern part of the Eurasian Continent were examined. The Arctic, the eastern part of the Eurasian Continent, the Sea of Okhotsk, and the Bering Sea were selected for the important airmass source regions by considering the monthly normals of surface air temperatures. By using the seasonal variations of the airmass stratifications, the year 1985 was divided into five stages. The airmass stratifications tend to change simultaneously. The schematic distribution of air masses and frontal zones in stage I : late October to late February, stage II : early March to the first half of April, stage III : second half of April to early June, stage IV : mid-June to late August, and stage V : early September to mid-October, are illustrated in Figs. 48-52.

In stage I, the boundary between the A air mass and the Pc_1 air mass is located around 70°N (Fig. 48). The Pc_1 air mass is colder than the A air mass during most of stage I, and the stratification of Pc_1 air mass is very stable. The southern boundaries of the Pc_1 and Pc_2 air masses are located around 60°N and 40°N, and the polar frontal zones are formed around these boundaries west of 100°E. The Pacific polar frontal zone is formed around the southern periphery of the Pc air mass outbreaks. In the A air mass, stable stratification can be seen below 850 mb throughout the year. The upper limit of the Pc air mass is about 700 mb.

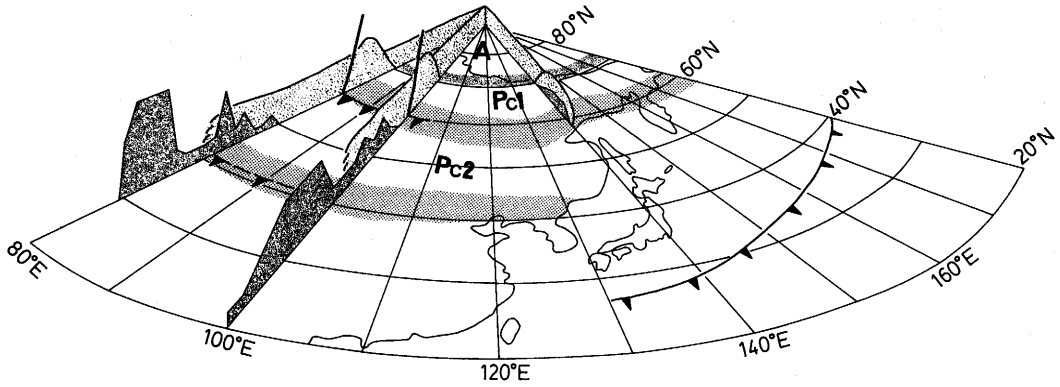

Fig. 48 Schematic model of air masses and frontal zones in the Arctic and the middle and high latitudes in the eastern part of the Eurasian Continent in stage I
Stipplings indicate the airmass boundaries, frontal marks (with solid and broken lines) indicate frontal zones (distinct and indistinct). Vertical profiles of air masses, frontal zones and topography are also shown.

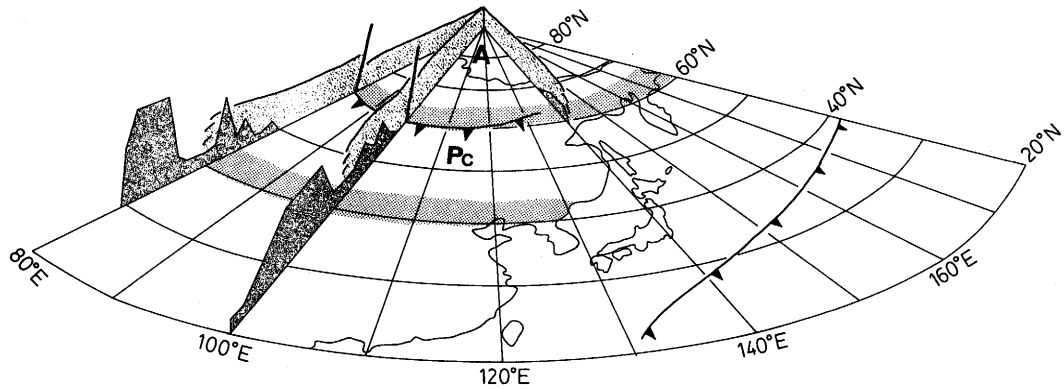

Fig. 49 As in Fig. 48, except for stage II

In stage II, the extent of the A air mass spreads to 60-65°N (Fig. 49). The Arctic frontal zone is formed at the southern periphery of the A air mass west of 140°E. The southern boundary of the Pc air mass, whose stratification is stable, is seen in 40°N over the continent. The Pacific polar frontal zone is seen over the ocean, whereas the Pm air mass does not exist in this stage. The upper limits of the A and Pc air masses are 700 mb and 850 mb, respectively.

In stage III, the southern boundary of the A air mass exists in 60-70°N and the Arctic frontal zone is formed west of 100°E (Fig. 50). The stratification of the Pc air mass becomes relatively unstable and its southern boundary is seen around 40°N over the continent. The Pm air mass exists in the Sea of Okhotsk and the Bering Sea. The Pacific polar frontal zone can be found to the south of the Pm air mass. The vertical extent of the A, Pc and Pm air masses are 700 mb, 700 mb and 850 mb, respectively.

In stage IV, the southern periphery of the A air mass is located in 65-70°N, and the Arctic frontal zone can be seen in 60-65°N (Fig. 51). A large $\nabla\theta e$ zone is seen in the Pc

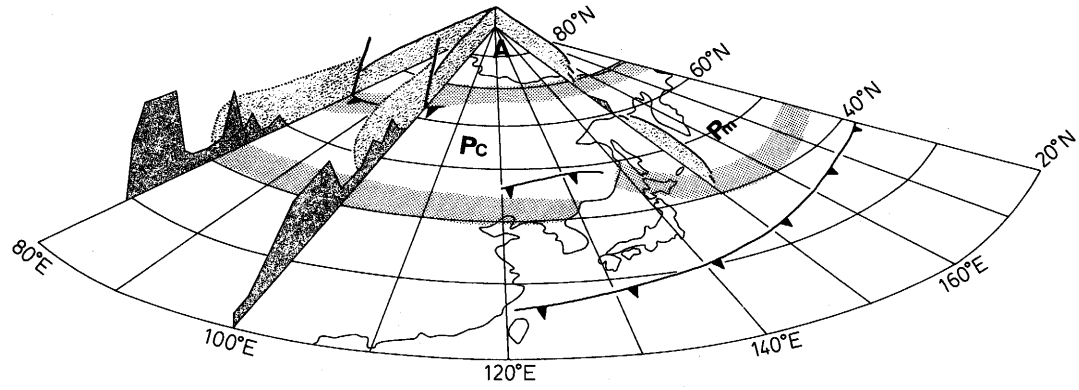

Fig. 50 As in Fig. 49, except for stage III

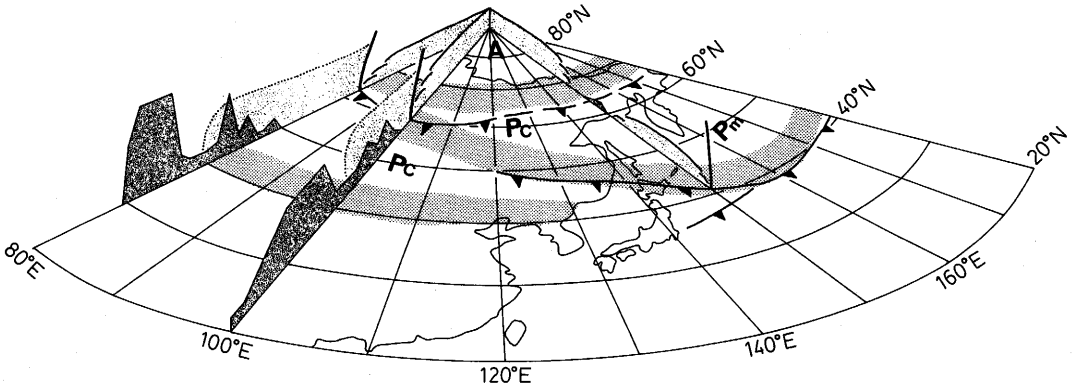

Fig. 51 As in Fig. 49, except for stage IV

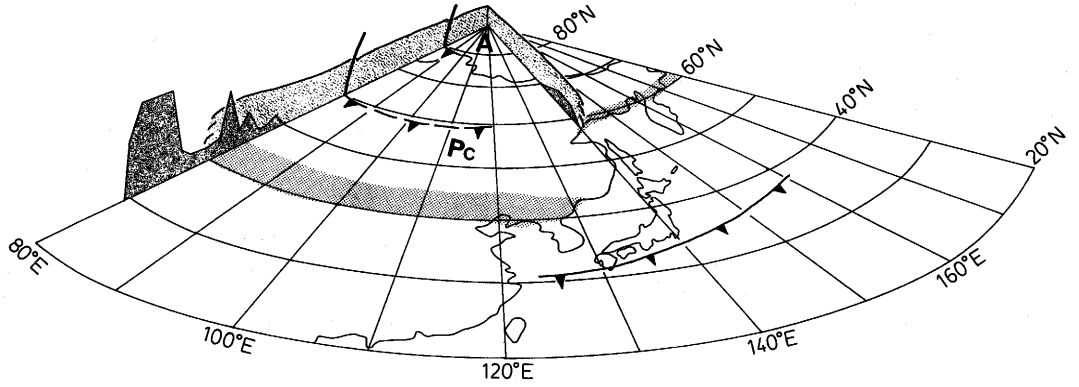

Fig. 52 As in Fig. 49, except for stage V

airmass source region (figures are not shown in this paper). The southern boundary of the Pc air mass exists around 40°N. The stratification of the Pc air mass is unstable and the moist air advection is observed in this stage. The Pm air mass is located around the Sea of Okhotsk and the Bering Sea, and the Pacific polar frontal zone is formed at the southern periphery of the Pm air mass. Upper limits of the A, Pc and Pm air masses are 850 mb, 700 mb and 850 mb.

In stage V, the boundaries of the air masses are generally indistinct (Fig. 52). The Arctic frontal zone is seen around 80°N west of 100°E and an indistinct polar frontal zone is found around 60°N. The stratification of the Pc air mass is stable, and its southern boundary is seen around 40°N west of 130°E and around 60°N east of 140°E. The Pacific polar frontal zone, whose occurrence frequency is the largest of all the stages, exists south of the Japanese Islands. Upper limits of the air masses cannot be identified, because of the linear vertical profiles of temperature and θe in the air masses.

It is worth noting that the stratifications and distributions of air masses in spring (stage II and III) are different from those in autumn (stage V). This difference may be due to the seasonal variation of sunshine duration and the different heat capacities between the continent and the ocean, and it should be investigated in the future.

Acknowledgments

I wish to thank Professor Ikuo Maejima of Nihon University for his continuous encouragement and advice. And I express my gratitude to Professor Michio Nogami, Professor Takehiko Mikami, Dr. Shuichi Oka, Dr. Yoshio Tagami and Dr. Keisuke Suzuki of Tokyo Metropolitan University, and Dr. Tohru Umemoto of Meiji University for their helpful suggestions.

I also thank Dr. Kuranoshin Kato of Water Research Institute, Nagoya University for his presentation of data used in this study.

References Cited

Arakawa, H. (1943): *Tenki-bunseki, Jou-kan (Weather Analysis, the First Volume).* Chijin-shokan, Tokyo, 487p.*

Barry, R. G. (1967): Seasonal location of the Arctic front over North America. *Geogr. Bull.*, **9**, 79-95.

——— and Chorley, R. J. (1987): *Atmosphere, Weather and Climate.* Methuen, London, 460p.

Bergeron, T. (1930): Richtlinien einer dynamischen Klimatologie. *Met. Zeit.*, **47**, 246-262.

Borchert, J. R. (1953): Regional differences in the world atmospheric circulation. *Ann. Assoc. Amer. Geogr.*, **43**, 14-26.

Brunnschweiler, D. H. (1957): Die Luftmassen der Nordhemisphäre. *Geogr. Helvetica*, **12**, 164-195.

Bryson, R. A. (1966): Air masses, streamlines, and the boreal forest. *Geogr. Bull.*, 8, 228-269.

Corcoran, W. T. (1987): Airmass climatology. *The Encyclopedia of Climatology.* Van Nostrand Reinholt Company, 986p.

Henderson-Sellers, A. and Robinson, P. J. (1986): *Contemporary Climatology.* Longman, New York, 438p.

Itokazu, M. (1972): Climate of Okinawa. *Tenki*, **19**, 231-242.*

Kanno, H. (1988): Polar air mass in the Bai-u season over East Asia. *Geographical Review of Japan*, **61**, 615-631.**

Kato, K. (1985): On the abrupt change in the structure of the Baiu front over the China Continent in late May of 1979. *J. Met. Soc. Japan*, **63**, 20-36.

——— (1987): Airmass transformation over the semiarid region around North China and abrupt change in the structure of the Baiu front in early summer. *J. Met. Soc. Japan*, **65**, 737-750.

——— (1989): Seasonal transition of the lower-level circulation systems around the Baiu front in China in 1979 and its relation. *J. Met. Soc. Japan*, **67**, 249-265.

Kawamura, T. (1973): *Monsoon Asia no shizen-kisetsu* (Natural seasons in Monsoon Asia). In Yoshino, M. M. (ed.) "*Monsoon Asia no Mizu-shigen (Water Resources in Monsoon Asia)*", Kokon-shoin, 227-244.*

Kikuchi, K. (1979): *Kyokuchi kishogaku, 1. Hokkyoku* (The meteorology in the polar region, 1. The North Pole). *Tenki*, **26**, 53-56.*

Kimachi, T. (1953): On the seasonal change of upper troposphere. *Kenkyu-Jiho*, **5**, 369-378.

Krebs, J. S. and Barry, R. G. (1970): The arctic front and the tundra-taiga boundary in Eurasia. *Geogr. Rev.*, **60**, 548-554.

Maejima, I. (1967): Natural seasons and weather singularities in Japan. *Geogr. Rept. Tokyo Metropl. Univ.*, No.**2**, 77-103.

Matsumoto, J. (1983): Wintertime location of the arctic frontal zones. *Geographical Review of Japan*, **56**, 624-638.**

——— (1988): Large-scale features associated with the frontal zone over East Asia from late summer to autumn. *J. Met. Soc. Japan*, **66**, 565-579.

Matsumoto, S., Ninomiya, K. and Yoshizumi, S. (1971): Characteristic features of "Baiu" front associated with heavy rainfall. *J. Met. Soc. Japan*, **49**, 267-281.

Ninomiya, K. and Muraki, H. (1986): Large-scale circulations over East Asia during Baiu period of 1979. *J. Met. Soc. Japan*, **64**, 409-429.

Nitta, T. (1988): *Shin-kisho-dokuhon (New Textbook of Meteorology), Dai II ki Kishogaku no Promenade 11 (The Meteorological Promenade in Second Term, No.11)*, Tokyodo-shuppan, 290p.*

Ogawa, H. (1987): *Tasai na nihon no kikou* (Colorful Japanese climate). In Matsui, K. and Ogawa, H. (ed.) "*Nihon no Fudo (Japanese Climate)*", Heibon-sha, 7-20.*

Palmén, E. and Newton, C. W. (1969): *Atmospheric Circulation Systems.* Academic Press, New York, 603p.

Petterssen, S. (1940): *Weather Analysis and Forecasting.* McGraw Hill, New York, 503p.

Reed, R. J. (1960): Principal frontal zones of the Northern Hemisphere in winter and summer. *Bull. Amer. Met. Soc.*, **41**, 591-598.

Saito, N. (1966): A preliminary study of the summer monsoon of southern and eastern Asia. *J. Met. Soc. Japan*, **44**, 44-59.

Saito, R. (1957): Climate of Japan and her meteorological disasters. *Geophy. Mag.*, **28**, 89-105.

Schumann, T. E. W. and van Rooy, M. P. (1951): Frequency of fronts in the Northern Hemisphere. *Arch. Met. Geoph. Biokl. (A)*, **4**, 87-97.

Sugimoto, Y. (1966): *Baiu-ki ni Okeru Ohohtsukukai Koukiatsu no Kentou (Examination of Okhotsk Anticyclone in the Bai-u Season). Kanto-Koshin Chihou Yohou Kentoukai Shiryou (Data of Examination Meeting for Forecasting in Kanto and Koushin Districts).**

Takahashi, K. (1942): Dynamical climatology in Japan. *J. Met. Soc. Japan (2nd S.)*, **20**, 171-181.*

Tamiya, H. (1986): Jahreszeitliche Gliederung der nordhemisphärischen Atmosphäre in synoptischklimatologischer Betrachtungsweise. *Geophys. Mag.*, **41**, 217-259.

Wendland, W. M. and Bryson, R. A. (1981): Northern Hemisphere airstream regions. *Mon. Wea. Rev.*, **109**, 255-270.

Willet, H. C. and Sanders, F. (1959): *Descriptive Meteorology (2nd. ed.)*. Academic Press, New York, 355p.

Yoshimura, M. (1967): Annual changes in the frontal zones in the Northern Hemisphere. *Geographical Review of Japan*, **40**, 393-408.**

Yoshino, M. M. (1963): Rainfall, frontal zones and jet streams in early summer over East Asia. *Bonner Meteorologische Abhandlungen*, Heft **3**, 1-126.

——— (1965): Four stages of the rainy season in early summer over East Asia (Part I). *J. Met. Soc. Japan*, **43**, 231-245.

——— and Fukuoka, Y. (1967): Pressure pattern calendar of East Asia. *Tenki*, **14**, 10-15.*

(*: in Japanese, **: in Japanese with English abstract)